LITHIUM EXTRACTION FROM GEOTHERMAL BRINE BY ADSORPTION METHOD WITH ELECTROLYTIC γ-MnO_2 SORBENT

A Thesis Submitted to
the Graduate School of Engineering and Sciences of
İzmir Institute of Technology
in Partial Fulfillment of the Requirements for the Degree of

MASTER OF SCIENCE

in Materials Science and Engineering

by
Seyra TOPRAK

July, 2022
İZMİR

ACKNOWLEDGEMENTS

First of all, I would like to express my special thanks to my advisor, Prof. Dr. Mustafa M. Demir, for his guidance, support, encouragement and insightful comments during the progress of my master's thesis and the writing process. I would like to thank my co-advisor Prof. Dr. Alper Baba for his contributions and support during my studies.

I am also thankful to the rest of my thesis defense committee, Prof. Dr. Fatma Nil Ertaş and Assoc. Prof. Aslı Yüksel Özşen for their valuable suggestions and comments.

I would especially like to thank to all Demir Lab Research group members Öykü Toker, Hürriyet Yüce Çakır, Berk Akgün and Çağlar Erdem for their support, assistance and friendship throughout my master’s studies. A special thank you to Öykü Toker for not only being a wonderful coworker but also a sincere friend who shares our dreams and concerns.

Endless thanks to my dear family, my father Hüseyin Toprak, my mother İlknur Toprak and my sister Sena Toprak for always believing in me, supporting and encouraging me. They were always by my side and went through this process with me.

Finally, special thanks to my love Çağlar Erbay, for always being there for me, motivating me to do my best and comforting me during my stressful times.

ABSTRACT

LITHIUM EXTRACTION FROM GEOTHERMAL BRINE BY ADSORPTION METHOD WITH ELECTROLYTIC γ-MnO_2 SORBENT

In recent years, studies on the recovery of lithium metal have attracted great attention due to its wide application areas, especially in lithium-ion batteries. Recovery of lithium from brines is preferred considering the environmental impacts in mining. The application of manganese oxide sorbents to recover lithium from geothermal brines has been extensively studied as it is a potential source of lithium. In this thesis, adsorption was performed in Tuzla Geothermal Power Plant (TGPP) at 87 °C and 2 bar using a mini-pilot system in the reactor near the reinjection well of the plant to investigate the adsorption performance in field conditions. As a new approach, electrolytic manganese dioxide (γ-MnO_2), which is widely used as cathode material in batteries, was used as the sorbent material for lithium and its adsorption/desorption performance was investigated.

Batch adsorption experiments were performed in synthetic lithium solution and the optimum working conditions were determined as pH 12, adsorbent concentration of 3 g/L, and initial lithium-ion concentration of 200 mg/L. The highest adsorption capacity of the sorbent in the Langmuir model was found as 9.74 mg/g. The maximum adsorption performance was obtained at 1h adsorption in Tuzla GPP. In the continuation of the study, desorption was carried out in acidic medium with the brine-treated sorbent. Lithium concentration was enriched to around 250 ppm with repetitive desorption studies. Reusability of the sorbent was investigated and the reused sorbent showed almost 40% performance compared to virgin powder. γ-MnO_2 was found as a promising sorbent for the separation of lithium from geothermal brines.

ÖZET

JEOTERMAL TUZLU SUDAN ADSORPSİYON YÖNTEMİ KULLANILARAK ELEKTROLİTİK γ-MnO_2 ADSORBANI İLE LİTYUM AYRIŞTIRILMASI

Son yıllarda özellikle lityum iyon pillerde geniş uygulama alanları nedeniyle lityum metalinin geri kazanımı ile ilgili çalışmalar büyük ilgi görmektedir. Madencilikteki çevresel etkiler göz önüne alındığında, lityumun tuzlu su kaynaklarından geri kazanılması tercih edilmektedir. Günümüzde, potansiyel bir lityum kaynağı olmasından dolayı, jeotermal tuzlu sulardan manganez oksit bazlı adsorbanları kullanılarak lityum iyonlarının geri kazanılması kapsamlı bir şekilde incelenmiştir. Bu tezde, saha koşullarında adsorpsiyon performansını araştırmak için Tuzla Jeotermal Santrali'nde (TGPP), tesisin reenjeksiyon kuyusunun yakınındaki reaktörde mini pilot bir sistem kurularak, 87 °C ve 2 bar'da adsorpsiyon gerçekleştirilmiştir. Yeni bir yaklaşım olarak, yaygın olarak pillerde katot malzemesi olarak kullanılan elektrolitik manganez dioksit (γ-MnO_2), lityum için adsorban malzeme olarak kullanılmış ve adsorpsiyon/desorpsiyon performansı araştırılmıştır.

Sentetik lityum çözeltisinde kesikli adsorpsiyon çalışmaları yapılmış ve optimum çalışma koşulları pH 12, adsorban konsantrasyonu 3 g/L ve 200 mg/L'lik başlangıç lityum iyon konsantrasyonu olarak belirlenmiştir. Langmuir modelinde adsorbanın en yüksek lityum adsorpsiyon kapasitesi 9,74 mg/g olarak bulunmuştur. Maksimum adsorpsiyon performansı sahada yapılan 1 saatlik adsorpsiyon sonucu elde edilmiştir. Çalışmanın devamında tuzlu su ile muamele edilmiş sorbent ile asidik ortamda desorpsiyon gerçekleştirilmiştir. Lityum konsantrasyonu, tekrarlayan desorpsiyon çalışmaları ile yaklaşık 250 ppm'ye kadar zenginleştirildi. Sorbentin yeniden kullanılabilirliği araştırıldı ve yeniden kullanılan sorbent, işlenmemiş toza kıyasla neredeyse %40 performans gösterdi. γ-MnO_2, lityumun jeotermal tuzlu sulardan ayrılması için umut verici bir sorbent olarak bulundu.

TABLE OF CONTENTS

LIST OF FIGURES

Figure **Page**

Figure **Page**

LIST OF TABLES

Table **Page**

CHAPTER 1

INTRODUCTION

Lithium is the lightest and 25th most abundant metal, and has a number of desirable properties, including high specific heat capacity, a high electrochemical potential of 3.04 V, and a low coefficient of thermal expansion.[1,2] The lithium element is never found in nature in its free form and is only found in compounds, primarily ionic compounds, due to its strong reactivity and flammability, which is common by other alkali elements.[3]

In recent years, due to their attractive physical and chemical characteristics, lithium compounds have been widely used in a variety of fields, including the glass and ceramics, lubricating greases, metallurgical industries, chemicals, pharmaceuticals, rubbers, and, most notably lithium-ion batteries.[4–6] Therefore, it is important to identify fast and efficient methods for separating, purifying and recovering lithium from its sources. Considering the gradual depletion of ores in mining and environmental impacts, it is preferable to recover lithium from brine solutions.[7,8] Geothermal brines contain high concentrations of minerals and are a source of various valuable elements, making it a potential source of lithium.[9] Lithium is industrially produced as a variety of compounds depending on the projected end-use application and processing techniques. The most commonly produced lithium compound is lithium carbonate (Li_2CO_3) (60%), which is then followed by lithium hydroxide (23%), lithium metal (5%), butyl lithium (4%), and lithium chloride (3%).[10]

Recently, a number of technologies have been developed to extract lithium from water sources. Among these technologies, adsorption has emerged as an ideal method for the separation of lithium, providing significant advantages such as wide availability, high efficiency, cheaper cost and simplicity in operation.[7] Currently, adsorption with metal oxides and hydroxides is the most studied and technically advanced method for the selective removal of lithium from brines, and among them, manganese oxide and titanium oxide derivatives are one of the most promising absorbent materials.[11] There are several known polymorphs of manganese oxides, including α-, β-, λ- and γ-MnO_2

which are widely employed as catalysts, electrode materials in Li-ion batteries and ion sieve adsorbents.[12] Most representatively, synthesis and application of spinel type λ-MnO_2 ion sieve adsorbents in the recovery of lithium ions from brines have been extensively studied.[13] The γ-phase of MnO_2 polymorphs is used in commercial alkaline batteries because of its capability to intercalate protons, hence, its lithium intercalation mechanism has also been investigated.[14]

In the thesis, as a new approach, this relatively inexpensive electrolytic manganese dioxide (γ-MnO_2), which is normally used as the cathode material in lithium-ion batteries, was used as an absorbent material for lithium. In the first stage, structural characterization of γ-MnO_2 powder was carried out using XRD, XRF, SEM, BET and DLS methods and the compatibility of the used powder with commercial γ-MnO_2 was examined. Afterwards, experiments were carried out using synthetic lithium solution to examine the adsorption performance of γ-MnO_2 powder, then an adsorption experiment was carried out in Tuzla geothermal power plant to see the adsorption performance under field conditions. The desorption performance of the powder was studied in an acidic environment.

CHAPTER 2

LITERATURE REVIEW

2.1. Lithium Supply/Demand

The lithium market is gradually expanding. Lithium production has increased rapidly in the last decade due to high demand for lithium in the production of lithium-ion batteries (LIBs). Since rechargeable LIBs are widely utilized in the rising market of portable electronics and especially in electric vehicles, lithium consumption for LIBs has increased exponentially in recent decades.[15] This have a major influence on lithium prices on the global market. In China, for instance, the price of lithium carbonate increased from $6,400 to $12,000 per/ton.[16]

Due to the projected development of these technologies, demand for lithium is expected to increase by up to 900 thousand tons per year by 2025 in the near future, which is three times more than about 300 thousand tons per year in 2018.[17] According to one of the latest estimates, lithium demand would reach 1.79 million tonnes per year by 2030, up from 317,000 tonnes presently, with the majority of the demand coming from the electric vehicle sector.[11] Electric vehicles are reported to account for 75 thousand tons of lithium consumption per year, or around 24% of world's total demand. Based on projections for increased production of electric vehicles employing LIBs, this is expected to climb to 1.42 million tonnes/year by 2030, accounting for 79 percent of overall demand.[18] While there are several reports from some companies, the data by BMO Capital Markets[19] is cited here in Figure 2.1.

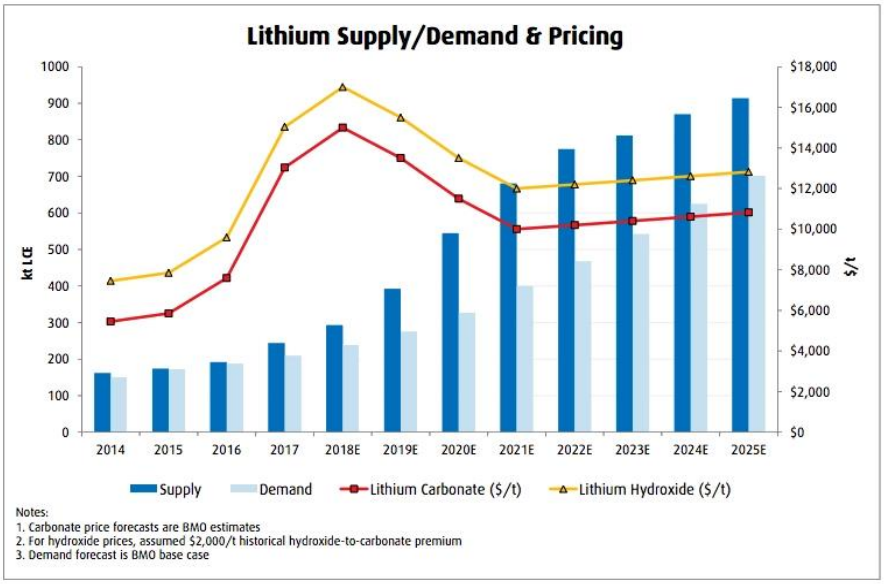

Figure 2.1. Lithium supply/demand and price.[19]

2.2. Application Areas of Lithium

According to the US Geological Survey's current data on global lithium resources in the end-use market[20], batteries accounted for the majority of lithium consumption in 2019 with 65%, followed by ceramics and glass industry with 18%, lubricating greases with 5%, production of polymers with 3%, while the remaining distributions are given in the Figure 2.2. below.

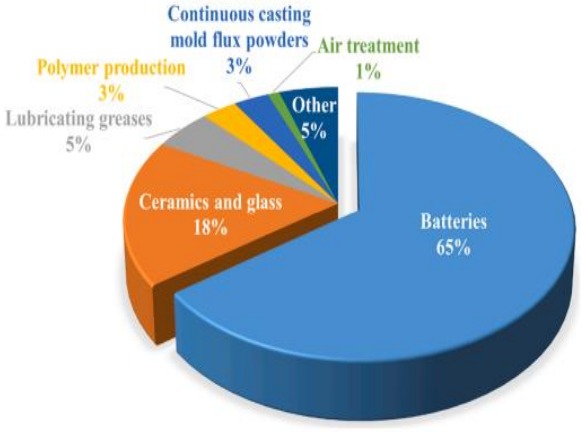

Figure 2.2. Distribution of lithium's numerous applications across the world in 2019.[21]

2.2.1. Lithium-ion Batteries

Today, lithium and LIBs make up approximately 37% of the world's rechargeable battery industry and their popularity is increasing day by day.[22] Due to its extremely high energy density and high electrochemical potential, lithium is used in rechargeable lithium ion batteries (LIBs).[2,23] Rechargeable LIBs are commonly used in mobile phones, computers, video cameras, electric vehicles, and grid storage applications.[24] LIBs are classified into two types as primary and secondary batteries. Secondary batteries are rechargeable while primary batteries are non-rechargeable.[25] In primary batteries, metallic lithium is used as the anode, while the electrolyte is a lithium salt dissolved in an organic solvent. In secondary batteries, lithium metal oxides such as $LiCoO_2$, $LiNiO_2$ and $LiMn_2O_4$ are used as the cathode, and as the electrolyte, an organic liquid dissolved with substances such as $LiClO_4$, LiBF4 and $LiPF_6$ are used. Primary batteries have a lithium concentration ranging from 0.60 g to 4 g, whereas secondary batteries have a lithium content ranging from 0.35 g to 26 g. [26]

Primary lithium batteries are most commonly used in cameras, calculators, computers, watches, electronic games, and other electronic devices, while secondary lithium batteries are mainly used in portable computers and mobile phones, video cameras, tablets, and electric vehicles.[26]

LIBs have excellent cycle life and extended life, high specific energy (230 Wh/kg), high power density (12 kW/kg), and exceptional charging and discharging efficiency, and these features have made LIBs the preferred technology for supplying energy to EVs and other portable electronic devices.[27,28] The supply and demand for electric cars are significantly impacted by LIBs since they are lighter, more compact, and more dependable than other types of rechargeable batteries now on the market. As a result, it is expected that the demand for LIBs will rise dramatically in the coming years.[10]

2.2.2. Other Applications

Ceramics and glasses are the second most common use of lithium after batteries. The use of lithium in glasses and ceramics improves a variety of product qualities, such as increasing the mechanical strength and decreasing the shrinkage in fine ceramics.[29] When lithium is utilized in ceramics, it lowers the melting temperature and increase fluxing power. As a result, it lowers the firing temperature and shorten the firing cycle time and enhances product quality, plant efficiency, and productivity. In glasses, lithium enhances the melting rate of glass by lowering the viscosity of the glass and lowering the melting temperature. According to the tests, the performance of the glass furnace can be enhanced by 6-17% with a small amount of lithium, such as 0.1-0.2%. [30]

Another important lithium end use is lubricating greases, with lithium greases accounting for approximately 65% of all lubricating greases. Greases mainly consist of lubricating oil, additives and thickeners. A metallic soap is used as a thickener, and lithium soap is one of them. Lithium greases are highly stable, do not degrade at high temperatures or harden at low temperatures, and have great water resistance, making them a good choice for the lubrication of mechanical systems.[31]

For the production of aluminum, Li_2CO_3 is used as an electrolyte additive in molten aluminum, as a result of which it increases the electrical conductivity and also lowers the melting point. In this way, metal yield is increased and fluorine emissions are reduced.[29] Furthermore, LiCl or LiBr are used in air handling and air conditioning systems because they can keep humidity levels constant.[32]

Lithium is used to form alloys with many metals, of which lead and aluminum alloys are the most important ones. While lead alloys are used in the bearings of railway wagons, aluminum alloys are used in the structural components of aircraft. Aluminum-lithium alloys are preferred by aircraft manufacturers due to their low weight and high stability properties.[33]

2.3. Lithium Resources

Lithium can be obtained from various natural sources, which are classified as solid and liquid sources. Solid sources are consist of mineral ores, clays and recycled waste lithium-ion batteries, while liquid sources are mainly salt lake brine, geothermal brine, and seawater.[34]

Almost all of the commercial lithium is currently produced from brines and high-grade lithium ores. The distribution of lithium in various resources is given in Figure 2.3. It is seen that, continental brines account for 59% of available lithium resources, followed by hard rock (25%), hectorite (7%), and geothermal brines (3%).[22] In 2019, global lithium resources were reported to be 80 million tons (Mt), with the majority of the resources located in the Bolivia (21 Mt), United States (6.8 Mt), Argentina (17 Mt), Chile(9 Mt), Australia (6.3 Mt), China (4.5 Mt), Congo (Kinshasa)(3 Mt), and Germany (2.5 Mt).[20]

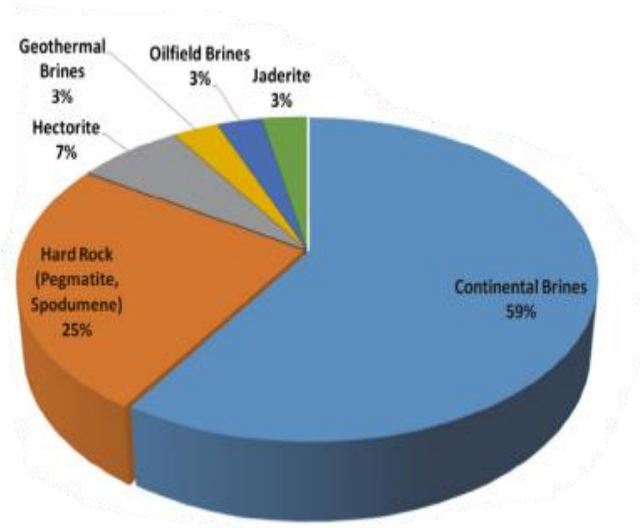

Figure 2.3. Distribution of lithium at various natural resources.[22]

2.3.1. Minerals/Clays

There are about 131 lithium minerals that are known, of which several silicates and phosphate-based minerals of economic importance, and have been investigated to exploit lithium values[23]. Table 2.1. shows some typical lithium-containing minerals and their lithium content[35]. At present, the majority of mineable minerals are found in

pegmatite environment, which are coarse-grained intrusive igneous rocks formed as a result of magma crystallization at depths in the crust. [36] Pegmatites include spodumene, lepidolite, eucryptite, petalite, and amblygonite, whereas hectorite and jadarite are claylike minerals. Australia, Canada, Zimbabwe, Portugal, and Brazil are the leading producers of lithium from hard rock ores. Greenbushes, located in Western Australia, is the world's largest lithium mine, producing high-grade lithium concentrate in the form of spodumene.[37]

Table 2.1. The most widely used Li-bearing minerals [3,35].

Mineral name	Formula	Li content % (w/w)
Spodumene	$LiAlSi_2O_6$	3.7
Lepidolite	$K(Li,Al)_3(Si,Al)_4O_{10}(F,OH)_2$	1.39-3.6
Petalite	$LiAlSi_4O_{10}$	1.6-2.27
Eucryptite	$LiAlSiO_4$	2.1-5.53
Amblygonite	$(Li,Na)AlPO_4(F,OH)$	3.4-4.7
Hectorite	$Na_{0.3}(Mg,Li)_3Si_4O_{10}(OH)_2$	0.54
Jadarite	$LiNaSiB_3O_7(OH)$	7.3

2.3.2. Brines

Lithium extraction from brines has attracted more and more attention as it is more environmentally friendly and cost-effective than extraction from ores.[38] The cost of producing lithium from salt lake brines is predicted to be US$2–3 kg^{-1}, compared to US$6–8 kg^{-1} from ores or spodumene.[39]

Seawater is the richest resource of lithium (approximately 230 billion tonnes), but the low lithium concentration (0.1–0.2 ppm) makes it unsuitable for technological applications.[40] Geothermal waters and oil-well brines both contain considerable levels of lithium.[22] Lithium concentrations range from 0.1 - 500 mg/L in several mineral-rich and hot geothermal brines.[6] Therefore, geothermal water is one of the most promising lithium resource from a technological standpoint. [41]

The ABC (Argentina, Bolivia, and Chile) area of South America is responsible to almost 70% of the world's lithium resources. Lithium concentrations range from 0.04-0.16 percent in the salars of Chile, Argentina, and Bolivia. Bolivia (resource: 9.0 Mt with 532 mg/L Li), Chile (resource: 2.6 Mt, 400-700 mg/L Li), and Argentina

(resource: 7.5 Mt, 1500-2700 mg/L Li) make up the next three countries in terms of brine deposits, which together make up about eighty percent of the global brine reserves.[4] In Table 2.2 below, the world's primary lithium-containing brine sources is listed, along with lithium concentrations and other typically observed metal concentrations.[42]

Table 2.2. The major lithium-containing brine resources.[42]

Source, Location	wt(%)				
	Li	Na	Mg	K	Ca
Salar de Atacama, Chile	0.157	9.1	0.965	2.36	0.045
Clayton Valley, USA	0.0163	4.69	0.019	0.4	0.045
Salton Sea, USA	0.01-0.04	5.0-7.0	0.07-0.57	1.3-2.40	2.26-3.9
Great Salt Lake, USA	0.0018	3.7-8.7	0.5-0.97	0.26-0.72	0.026-0.04
Salar de Uyuni, Bolivia	0.0321	7.06	0.65	1.17	0.0306
Hombre Muerto, Argentina	0.068-0.121	9.9-10.3	0.018-0.14	0.24-0.97	0.019-0.09
Zabuye Salt Lake, China	0.0489	7.29	0.0026	1.66	0.0106
Taijinaier, China	0.031	5.63	2.02	0.44	0.02

Although brines are the significant sources of lithium today, they contain several ions along with lithium, making it difficult to selectively recover lithium from brine sources. These co-existing ions include Mg^{2+}, Ca^{2+}, K^{+} and Na^{+}, among which brines are typically rich in Mg^{2+}. Therefore, it is necessary to separate lithium from other coexisting ions, in order to extract high-purity lithium products from brines. Li^{+} and Mg^{2+} are more difficult to separate than other ions because they have comparable chemical properties and ionic hydration radii. For comparison, lithium has an ionic radius of 0.79 angstrom (Å) and magnesium has an ionic radius of 0.72 Å.[11] Due to the complexity of process, magnesium/lithium ratio (Mg/Li ratio) is important in brine deposits. Hence, there are ongoing studies about recovering lithium from brines with high Mg/Li ratios.[43]

2.3.2.1. Lithium in Geothermal Brines

Lithium-rich geothermal brines have been identified as a potential domestic supply of lithium. Geothermal fluid is a hot and concentrated salt solution that has been enriched with Li, K and B elements by circulation through extremely hot rocks. To put it another way, geothermal energy is used for the energy-consuming process of extracting lithium from the rocks.[44] Recovery of lithium from geothermal brines has several advantages. There are no expenses or negative environmental impacts related with ore mining and physical processing. Also, because of ore minerals are already in solution, there are no costs involved with their dissolution into an aqueous phase. Even low-lithium brines are an important resource since geothermal waters process hundreds of m^3 of brine every hour and contain low but considerable amounts of Li^+.[9] The figure below gives the comparison of lithium extraction applications from geothermal brines with extraction from other sources in terms of their negative effects on environmental factors.

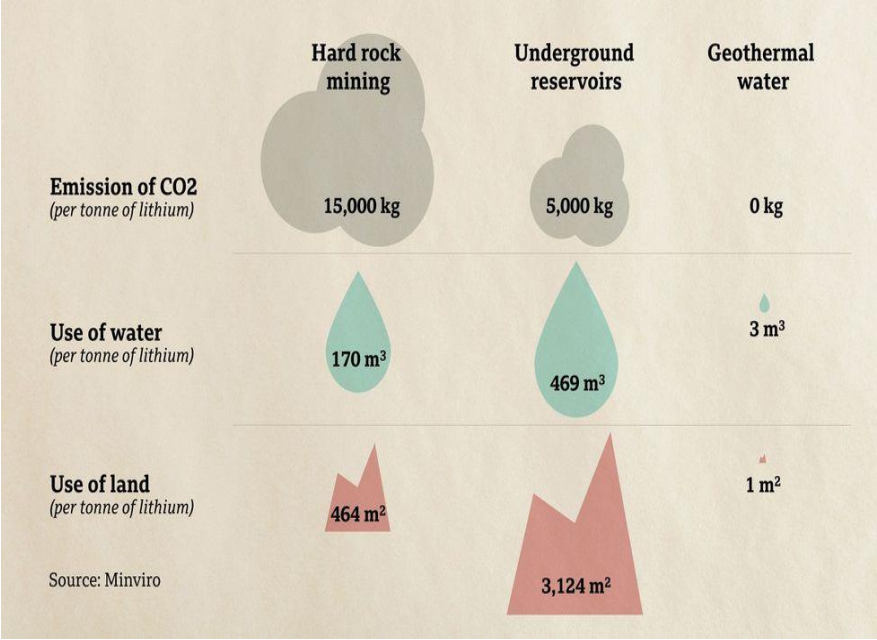

Figure 2.4. Comparison of the environmental impacts of lithium extraction from different sources.[44]

As an example, in a geothermal power plant in Salton Sea, USA, the recovery and recycling of lithium chloride from geothermal brine results in the production of

around 15 thousand tons of lithium salt per year. As a result, geothermal brine solutions are a significant source of lithium and have the potential to produce lithium salts that are cost-effective.[45] However, the complex chemistry, high salt content, and high temperatures of lithium-rich geothermal brines create challenges for the economic extraction of lithium.[11]

Turkey is positioned in the Alpine-Himalayan folds, and owing to its favorable geological conditions, Turkey possesses rich geothermal resources. In Turkey, there are over 1000 geothermal and mineral water resources. In 170 of these geothermal resources, the temperature is above 40 °C. The location of geothermal fields is 78% in Western Anatolia, 9% in Central Anatolia, 7% in Marmara region, 5% in Eastern Anatolia and 1% in other regions.[46] The Çanakkale-Tuzla geothermal field on Turkey's Biga Peninsula is important since it contributes to Turkey's energy generation and has a comparatively high lithium concentration of roughly 25 ppm. The facility is also the 30th largest geothermal power plant in Turkey.[47]

Figure 2.5. shows the lithium potential in the geothermal fields in Turkey while the Table 2.3 below gives the concentration of several existing ions taken from the retention pond of the Tuzla geothermal power plant.

Table 2.3. Ion concentration of Tuzla geothermal brine.[48]

Atom No	Element	ppm (mg/L)
3	Li	24.1
5	B	21.8
11	Na	25450.0
12	Mg	104

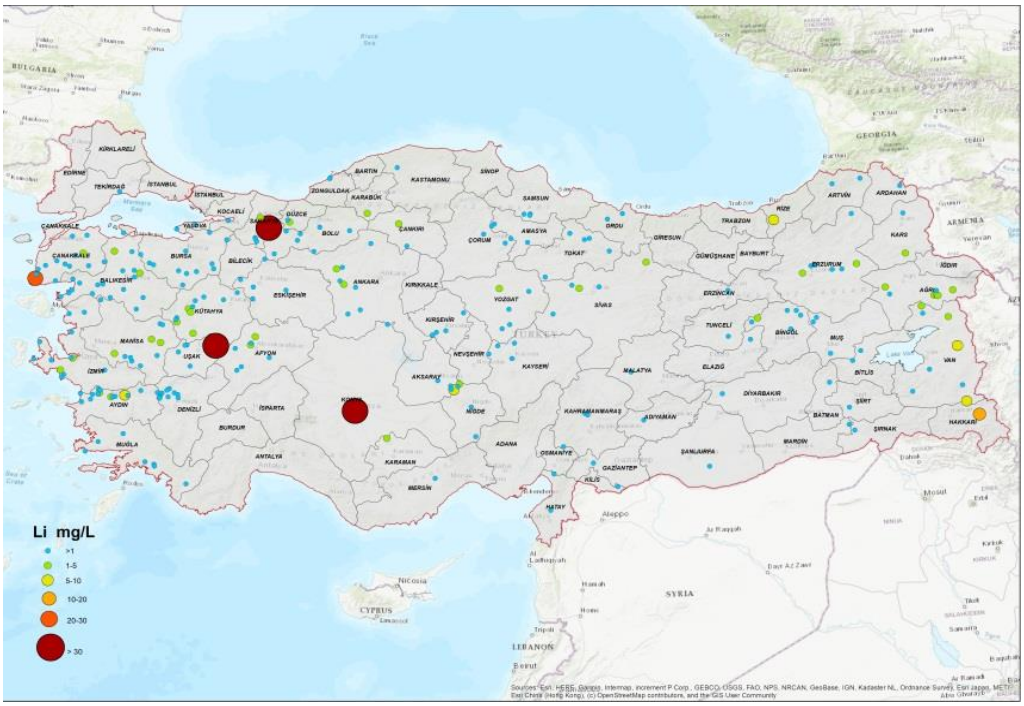

Figure 2.5. Lithium Potential in Geothermal Systems in Turkey.[49]

2.4. Methods for Lithium Extraction from Brines

There are numerous techniques that have been developed and extensively studied for the extraction of lithium from brines, including precipitation, adsorption, solvent extraction, ion exchange, and membrane processes.[50] Among the several techniques listed above, the adsorption method gives significant economic and environmental advantages for extracting lithium from brine with a high ratio of Mg/Li and low Li^+ concentration.[51] The process is relatively simple, with low energy consumption, high recovery rate, and high selectivity to lithium.[2]

2.4.1. Chemical Precipitation

Chemical precipitation is used to separate heavy metal ions from aqueous solutions with the addition of precipitating agents. In this process, the chemical reaction between the soluble metal compounds and the precipitating reagent converts the

dissolved metals into an insoluble form of metal hydroxides, sulfides or carbonates. Afterwards, filtration and/or settling is used to remove the precipitates from the solution. The amount of ionic metals present, the precipitants used, reaction conditions (particularly pH), and the presence of other components are all factors that influence the precipitation.[52] The flowsheet of the two-stage precipitation process used for the lithium recovery from Uyuni salar brine is shown in Figure 2.6. At the beginning of the precipitation process, the lithium-rich brine is subjected to a series of solar pond evaporations to obtain a concentrated brine. Lime ($Ca(OH)_2$) is then added to remove magnesium as $Mg(OH)_2$, and sulfate as $CaSO_4$. Then in the carbonation process; lithium reacts with Na_2CO_3 to produce technical-grade %99.6 Li_2CO_3.[4] This process, however, is unsuitable for brines with a high Mg^{2+}/Li^+ ratio, which makes lithium extraction challenging. Furthermore, this process produces large volumes of sludge, uses lots of chemicals and takes a long time to complete.[34]

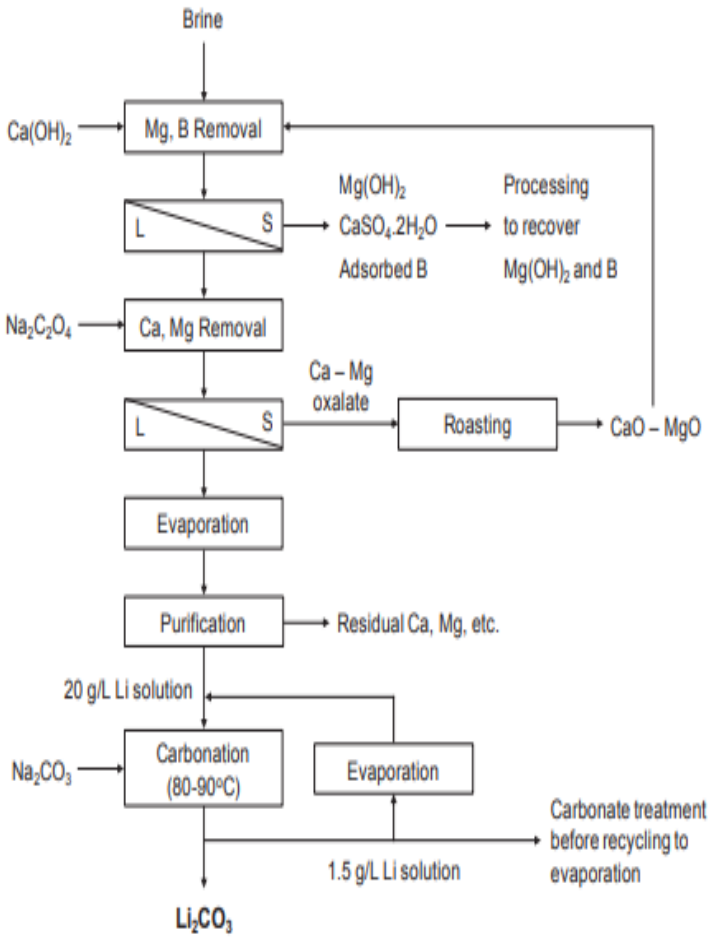

Figure 2.6. Flow sheet for lithium recovery from Salar de Uyuni brine.[50]

2.4.2. Solvent Extraction

One of the most popular techniques for removing metal ions from brines is solvent extraction, usually referred to as liquid-liquid extraction. In this procedure, an organic solvent containing an extractant (eluent) is combined with an aqueous metal salt solution, and the metal ions migrate from the aqueous to the organic phase after forming a hydrophobic combination with the extractant. The complex's affinity for the aqueous phase over the organic phase, as well as the complexes' relative solubility in both phases, are what lead to this migration.[53]

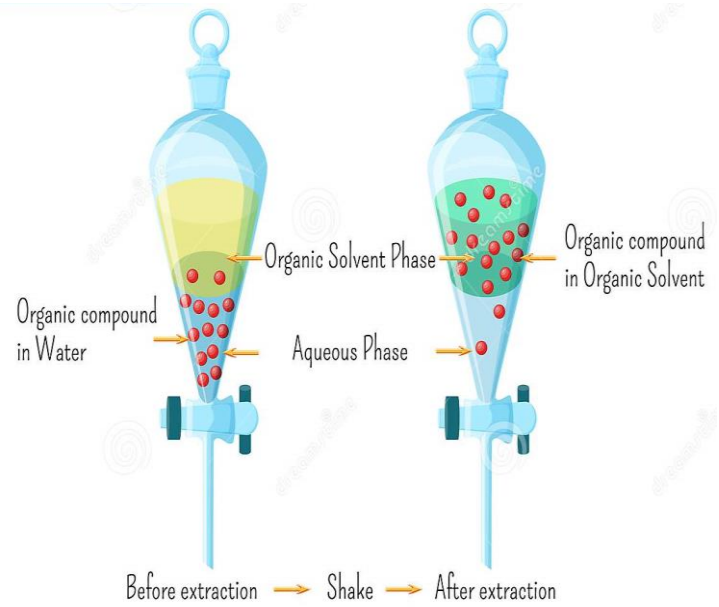

Figure 2.7. Schematic Representation of the Solvent Extraction Process[54].

The solvent extraction methods studied for lithium extraction from brines fall into three basic groups as: crown ether systems, multi-component systems including an extractant, a co-extractant, and a diluent, and ion liquid systems. An aqueous stripping agent, typically an acidic solution such as HCl, is then used to recover the metals that have been extracted into the organic phase.[1,11,55] Currently, Tributyl phosphate (TBP) / kerosene and ferric chloride ($FeCl_3$) is one of the most commonly used solvent extraction systems for the extraction of lithium ions.[56–59] $FeCl_3$ works as a co-extraction agent in this system, where it is critical for extracting lithium ions.[60,61] Tributyl

phosphate (TBP) is one of the most widely used neutral organophosphorus extractants while kerosene is a common diluent. [59] However, there are some disadvantages of using solvent extraction method for lithium recovery such as, using large quantities of organic solvents as an extractant corrodes process equipment and damages the environment. Therefore, it is important to develop sustainable technologies for lithium extraction from aqueous systems.[34]

2.4.3. Ion Exchange

The ion exchange method is one of the methods used today to separate lithium from brines. The metal ions in solution are reversibly exchanged with the ions in a solid ion exchange material during the chemical process known as ion exchange. Strong or weak cation and anion exchangers are the two major categories under which ion exchange resins belong.[62] The schematic representation of ion exchange process for removal of metal ions is shown in Figure 2.8.

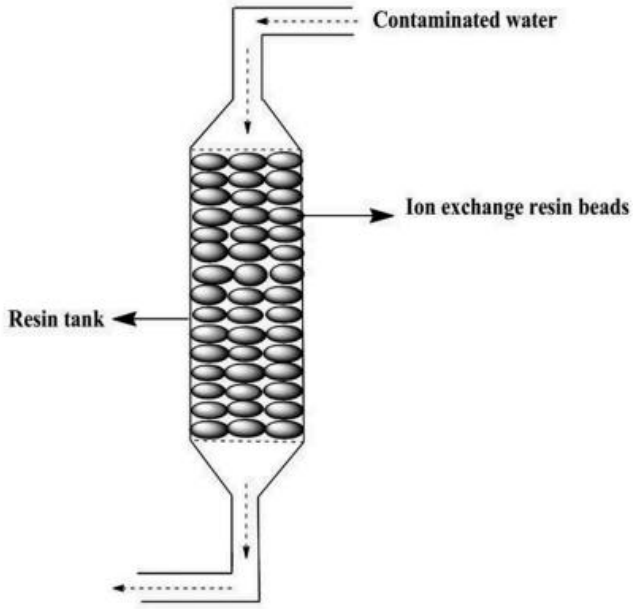

Figure 2.8. Schematic representation of ion exchange process [63].

Polystyrene sulfone cation exchangers and strongly basic anion exchangers are two types of ion exchangers that are commonly used.[62] The ion exchange process has

the drawbacks of being strongly influenced by solution pH and cannot be applied on a large scale. Also, synthetic resins are inherently costly.[63]

2.4.4. Adsorption

Adsorption can simply be defined as a mass transfer process in which the metal ion is transferred from the liquid phase to the surface of the solid and bonded by physical or chemical interactions.[64] Adsorbent refers to the surface on which adsorption takes place, whereas adsorbate refers to the molecular species that is adsorbed on it. The desorption process is the opposite of adsorption, which results in the release of the adsorbate from the surface. The schematic representation of the adsorption/desorption process is given in the Figure 2.9. below.

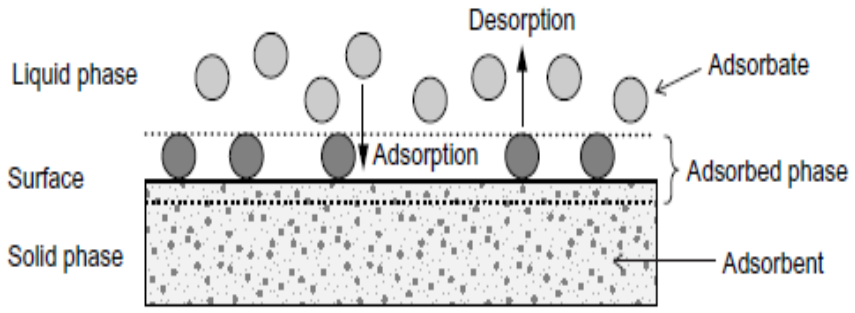

Figure 2.9. Schematic representation of adsorption/desorption process.[65]

Adsorption process is divided as physical and chemical adsorption according to the interaction forces between the adsorbate and adsorbent. Physical sorption occurs as a result of weak Van der Waals forces. In physical adsorption electrostatic forces occur including dipole-dipole and dispersion interactions, as well as hydrogen bonding between the adsorbate and the adsorbent. While in chemical adsorption stronger electrostatic forces such as covalent or electrostatic chemical bond occurs between adsorbent and adsorbate.[66]

The adsorption mechanism from the aqueous phase onto an adsorbent consists of three steps, as shown in the figure below:

(1) Film diffusion takes place, that is, the movement of a solute from a bulk solution to the adsorbent's surrounding film.

(2) The solute transported into the film moves to the pores of the adsorbent by internal diffusion.

(3) In the last stage, the adsorbate is adsorbed on the outer surface of the adsorbent by binding of the ions to the active sites.[67]

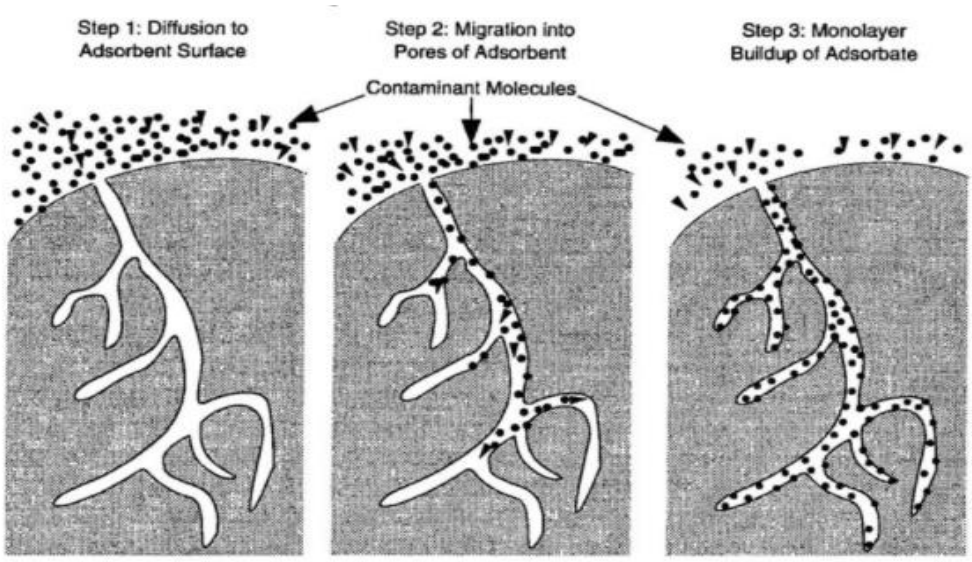

Figure 2.10. General mechanism of adsorption process.[68]

2.5. Lithium Extraction from Brine by Adsorption Method

Among the methods used in the process of selectively removing lithium from brines, adsorption has shown to be a good method of extracting lithium, with several advantages including availability, cheaper cost, profitability, efficiency, and simplicity of use. Various Li^+ adsorbent materials have been previously reported for lithium removal, including aluminum salt adsorbents, natural ores and carbon materials and manganese oxide based adsorbents.[7,69]

2.5.1. Manganese Oxides

Manganese oxides (MnO_2) are essential functional metal oxides used in a variety of technological applications including catalysts, hazardous metal adsorbents, ion-sieves, electrochemical battery electrodes (primarily lithium-ion batteries), and electrodes for supercapacitors.[70] Currently, manganese oxide-based ion sieves are recognized as the most promising adsorbents for lithium in industrial applications.[71] In aquatic environments, manganese oxides have many binding sites that are covered in surface hydroxyl groups, protons, and coordinated water molecules. They also have a high surface area and a microporous structure. Due to the hydroxyl groups on their surfaces, their surface charges vary according to pH values. They generally have a negative surface charge and therefore have a high adsorption capacity for metal ions. Consequently, they are commonly used as lithium adsorbents.[72]

There are several crystallographic polymorphs of manganese oxides (MnO_2) in nature. These polymorphs differ from one another in terms of their structural characteristics. Due to the way [MnO_6] octahedra are linked together by corner or edge sharing, tunnels or interlayers with various sizes of gaps occur. The number of cations or protons intercalated or extracted from the MnO_2 lattice is thought to be strongly governed by either the size of the tunnel or the interlayer spacing between sheets of [MnO_6] octahedra. n The following are the major manganese dioxide polymorphs: pyrolusite or β-MnO_2 (1×1 tunnel), hollandite or α-MnO_2 (2 × 2 tunnel), nsutite or γ-MnO_2 (2×1/1×1 tunnels), ramsdellite or R-MnO_2 (2×1 tunnel), birnessite or δ-MnO_2 (layered) and λ-MnO_2 (spinel/ with 3D pores), where (mxn) represents the tunnel dimensions.[14] Their selectivity for various ions or electron transfer kinetics is quite high due to their unique crystal structure.[14]

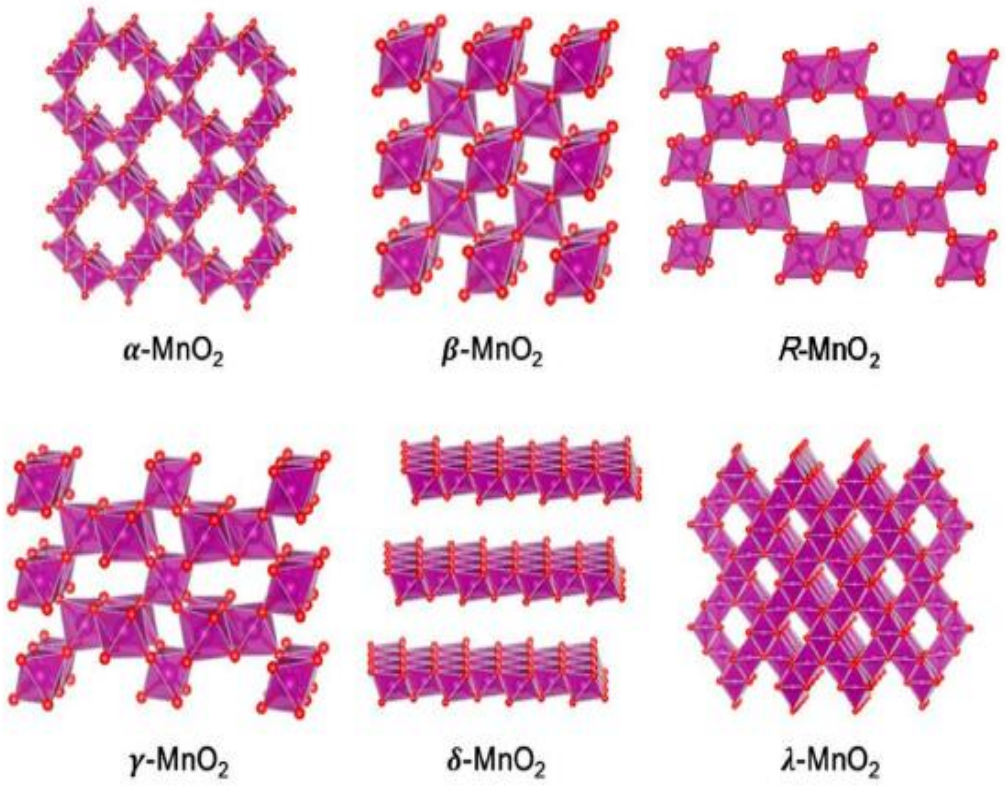

Figure 2.11. Crystal structures of α-, β-, R-, γ-, δ-, and λ- polymorphs of MnO_2.[14]

The schematic representation of α-, β-, R-, γ-, δ-, and λ- polymorphs of manganese oxide which vary in chain and tunnel (m×n) structures shown in Figure 2.11, while the crystallographic data of these major tunnel and layered manganese oxides given in Table 2.4.

Table 2.4. Crystallographic data of tunnel and layered manganese oxides.[73]

Crystallographic form	**Mineral**	**Crystal Symmetry**	**Lattice parameters (Å)**	**Features (Tunnels)**
R-MnO_2	Ramsdellite	Orthorhombic	a = 4.53; b = 9.27; c =2.87	(1 × 2)
β-MnO_2	Pyrolusite	Tetragonal	a = 4.39; c = 2.87	(1 × 1)
α-MnO_2	Hollandite	Tetragonal	a = 9.96; c = 2.85	(2 × 2)
γ-MnO_2	Nsutite	Complex tunnel(hex)	a = 9.65; c = 4.43	(1 × 1)/ (1 × 2)
λ-MnO_2	Spinel	Cubic	a = 8.04	(1 × 1)

2.5.1.1. Lithium-manganese oxide ion sieves

The most promising adsorbent is lithium ion-sieve (LIS), which has the following characteristics: low toxicity, cheap cost, good chemical stability, and high Li+ absorption capacity.[12,74] Lithium manganese oxides (LMO) and lithium titanium oxides (LTO) are the two main categories for LIS. Because of its high lithium selectivity, significant lithium adsorption capacities, and great regeneration performance, the LMO-type lithium-ion sieve is the most favored lithium adsorbent.[75]

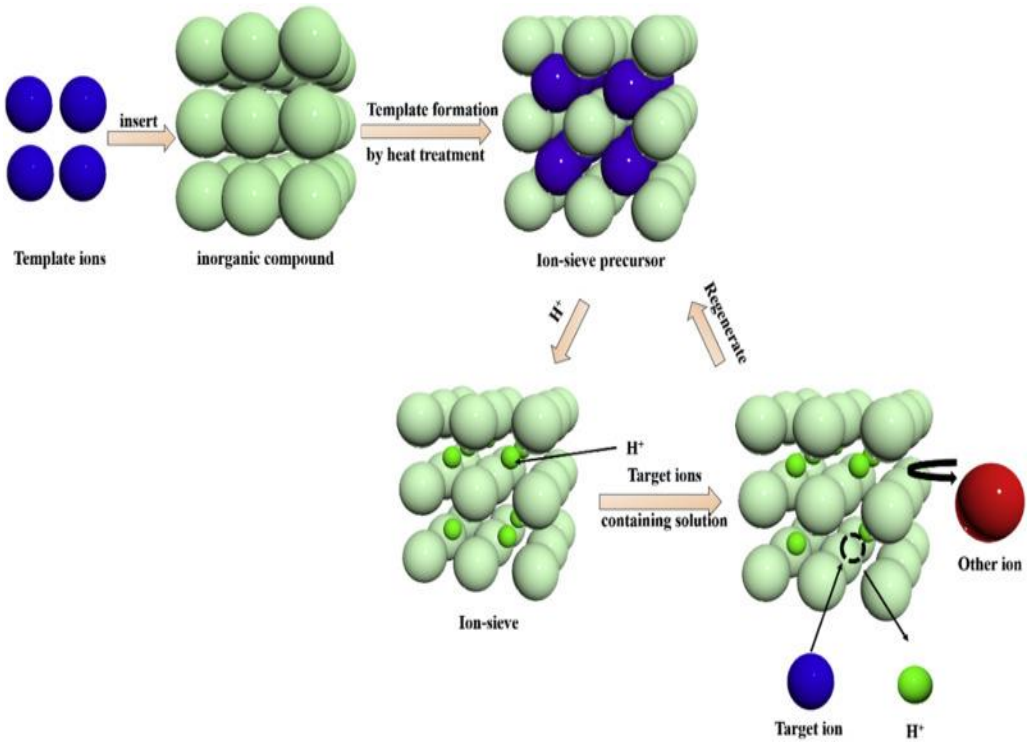

Figure 2.12. Ion Sieve effect.[69]

The template ions in the tunnels and interlayer gaps must be eliminated by a topotactic extraction process with acid in order to get manganese oxide ion-sieves. Following the extraction process, a topotactic reaction allows metal ions to re-enter the tunnels and interlayer spaces. In the removal and insertion of metal ions, there are two different types of reactions. The first is a redox-type reaction, while the second is an ion-exchange type reaction.[76] Therefore, LIS adsorbents have specific crystal sites that could only allow ions with ionic radius of smaller or equal to that of the target ions structure. The template ions have a screening and memory function that allows them to

adsorb target ions from the presence of several other ions. Lithium has the smallest ionic radius among all metal ions and because of that only lithium ion can enter the vacancy for lithium-ion sieve adsorbents[69,75]

Several manganese oxide type have been investigated as lithium-ion sieves, including, λ-MnO_2, $MnO_2 \cdot 0.3H_2O$, and $MnO_2 \cdot 0.5H_2O$, which are derived from $LiMn_2O_4$, $Li_{1.33}Mn_{1.67}O_4$, and $Li_{1.6}Mn_{1.6}O_4$, respectively.[77] Their theoretical lithium adsorption capacities from the aqueous solutions are summarized in Table 2.5.

Table 2.5. Theoretical adsorption capacities of the mainly used lithium ion-sieves[69]

Precursor	Ion-sieve	Theoretical adsorption capacity
$LiMn_2O_4$	λ-MnO_2	39.9 mg/g
$Li_{1.33}Mn_{1.67}O_4$	$MnO_2.0.3\ H_2O$	59.5 mg/g
$Li_{1.67}Mn_{1.67}O_4$	$MnO_2.0.5\ H_2O$	72.8 mg/g

The molar ratio of Li/Mn in various precursors affects the theoretical adsorption capacity of various adsorbents. Theoretical adsorption capacity typically increases with the Li/Mn molar ratio of the precursor. The largest theoretical adsorption capacity is found in $MnO_2.0.5H_2O$, whose precursor $Li_{1.67}Mn_{1.67}O_4$ has a Li/Mn molar ratio of 1:1.[69]

Manganese oxide sorbents has been synthesized, characterized, and investigated for lithium adsorption under different conditions. A variety of modifications have enhanced lithium sorption capacity. For example, Wang et al[78] synthesized λ-MnO_2 ion sieve by acidification of spinel $LiMn_2O_4$ with nitric acid and obtained that the ion-sieve has a high Li^+ sorption capacity of 30.9 mg/g specifically at pH=13, in 10mmol/L LiCl solution and the ion sieve was selective for Li-ion. In another study, Yang et al.[79] synthesized $LiMn_2O_4$, eluted Li^+ with acid, and obtained λ-MnO_2 with an adsorption capacity of 24.7 mg/g in Li^+ solution at pH 10. Furthermore, the lithium selectivity was found to be significantly greater than that of magnesium, implying that λ-MnO_2 could be used to extract Li^+ from brine or saltwater with a high Mg^{2+}/Li^+ ratio.

However, the actual performance of manganese oxides under real conditions for complex solutions might be lower than the experimental sorption capacity values obtained in synthetic solutions. As an example, Wang et al.[80] synthesized a variety of manganese oxides, including $LiMn_2O_4$, $Li_{1.66}\ Mn_{1.66}O_4$, and $Li_4Mn_5O_{12}$, and tested them

for selective recovery of lithium from geothermal water. The powdered $Li_4Mn_5O_{12}$ was shown to perform best for low lithium concentrations, however when tested against real geothermal brines, only had a maximum adsorption capacity of 8.98 mg/g.[80]

The adsorption characteristics of lithium ion-sieves are now mostly studied using an ion exchange mechanism. Li^+ intercalation and deintercalation in LMO-type LIS are said to follow an ion exchange process, according to Shen and Clearfield [81]:

$$LiMn_2O_4 + H^+ \rightarrow HMn_2O_4 + Li^+ \quad (2.1)$$

Lithium ions in solids can be completely replaced by protons through this process, although the sites of Mn^{3+} and Mn^{4+} in crystals remain constant during Li^+/H^+ ion exchange. It also exhibits good selectivity and excellent renewability for Li^+ because the spinel structure is maintained. Furthermore, the ion sieve's adsorption capacity increases as the pH of the solution rises, indicating the presence of an ion exchange process.[69]

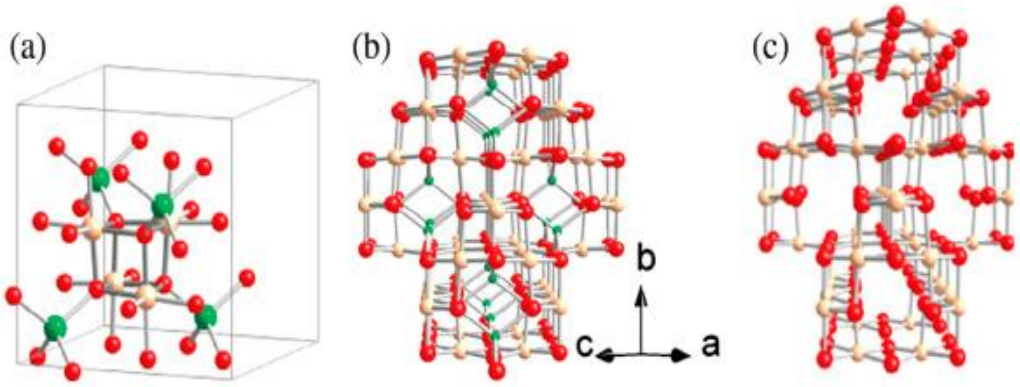

Figure 2.13. Representation of (a) the spinel $LiMn_2O_4$ unit cell, (b) the structure of the three-dimensional $LiMn_2O_4$ framework, and (c) the structure of λ-MnO_2 with voids after Li^+ extraction.[69]

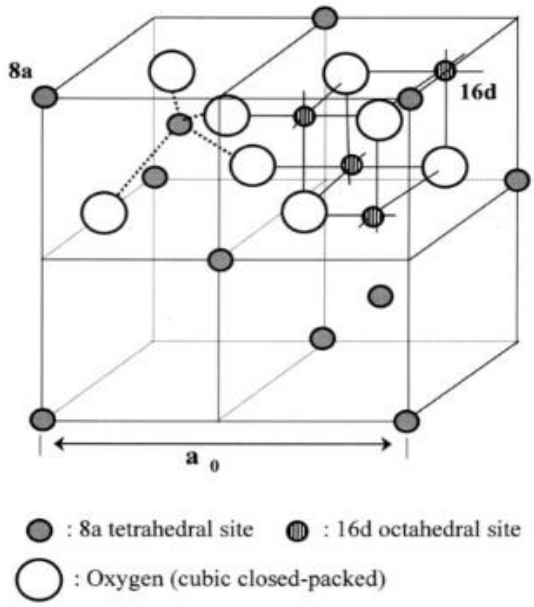

Figure 2.14. Structure of spinel-type lithium manganese oxide.[76]

The λ-MnO_2 (HMO) sorbent is obtained by the extraction of Li^+ ions from the $LiMn_2O_4$ (LMO) adsorbent precursor. After the lithium-ion is extracted by acidification, a gap as same as the size of lithium-ion is obtained without any damage in the structure. Therefore, the resulting λ-MnO_2 contains regular vacancies. In order to create a cubic-close-packed array, oxygen atoms occupy the 32e sites. manganese atoms and some lithium atoms share the octahedral 16d sites, and the other Lithium atoms occupy the tetrahedral 8a sites. Figure 2.13 and 2.14 above shows the spinel structure of $LiMn_2O_4$ (LMO). In Figure 2.13, Li, Mn, and O atoms are given with the colours of green, pink, and red, respectively. The spinel-type ion-sieves have an effective pore radius of around 0.7Å, which makes them selective for the adsorption of lithium and manganese oxides.[11]

2.5.1.2. Electrolytic Manganese Dioxide (γ-MnO_2)

Electrolytic manganese dioxide (EMD), is one of the cathode materials that is most frequently employed for alkaline batteries which has zinc and manganese dioxide as electrodes, the lithium–manganese dioxide primary batteries and supercapacitors. Due to its low manufacturing cost, environmental friendliness, strong redox potential,

greater relative performance across a wide temperature range, and extended storage life, this material is gaining more and more attention.[82]

The crystal structure of electrolytic manganese oxide (EMD) is intimately associated with the ε-, β- and γ-polymorphs of MnO_2, so it may contain these phases in the structure. γ-MnO_2, also referred to as nsutide MnO_2, is one of the best materials for battery applications and can be synthesized both chemically and electrochemically.[83] The structure of γ-MnO_2 is thought to be an irregular intergrowth of both ramsdellite (R-MnO_2) and pyrolusite (β-MnO_2) polymorphs.[84] The γ-MnO_2 polymorph is said to have a main ramsdellite structure with varied degrees of pyrolusite intergrowth including micro twinning imperfections. According to Ruetschi[85], another notable feature of γ-MnO_2 is the existence of cation vacancies and protons in the structure. According to Ruetschi, vacancies exist in -MnO_2 and each vacant Mn^{4+} site is connected to four protons in Hydroxyl form (OH^-) to balance the charge of manganese ions. These protons are referred to as "Ruetschi protons," and they are localized in the empty octahedra.[86]

The intergrown structure of γ-MnO_2 polymorph is given in Figure 2.15. The purple and yellow [MnO_6] octahedrons shown in the illustration, while the red spheres symbolize oxygen atoms and the locations of (1x1) and (2x1) tunnels represented with arrows.[87]

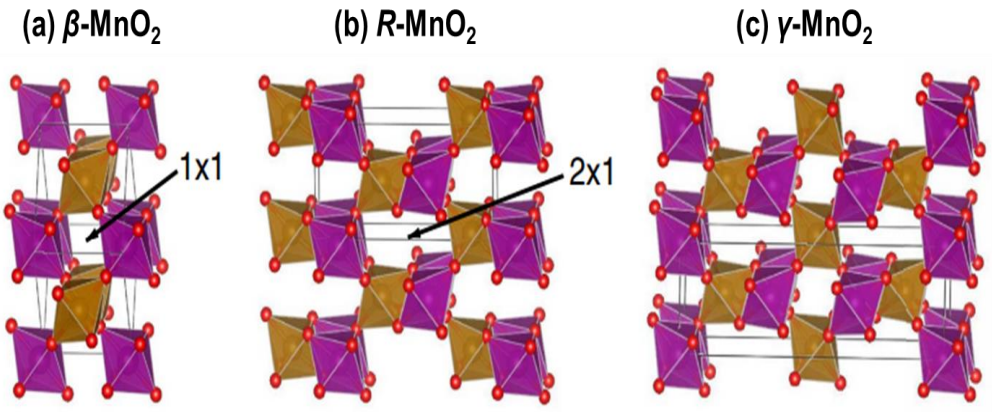

Figure 2.15. Schematic representation of the γ-MnO_2 structure in which (a) pyrolusite and (b) ramsdellite (R-MnO_2) is intergrown to form (c) γ-MnO_2.[87]

The tunnels in γ-MnO_2 structure (1x1)(2x1), has a size of 1.89, 2.3 Å, meaning that the lithium ion with ionic radius of 0.6Å, could be intercalated into the tunnel vacancy.[88]

In the study of Minakshi et al.[89], the electrochemical discharge of γ-MnO_2 in aqueous LiOH and (KOH) medias was studied, and the intercalation mechanism of lithium was investigated. It was observed that rectangular tunnels in the γ-MnO_2 structure accept lithium ions (Li^+) of comparable size to Mn^{4+}, followed by columbic interactions, and thus the structure is stable after the intercalation/extraction of lithium ions.

In another study, Jung et al[86] proposed that, the lithium-ion is positioned in the center of a regular octahedron composed of six adjacent oxygen atoms, with the assumption that all O-Li distances should be equal to 1.9 A°. Figure 2.16 (b) represents the model of a lithiated structure.

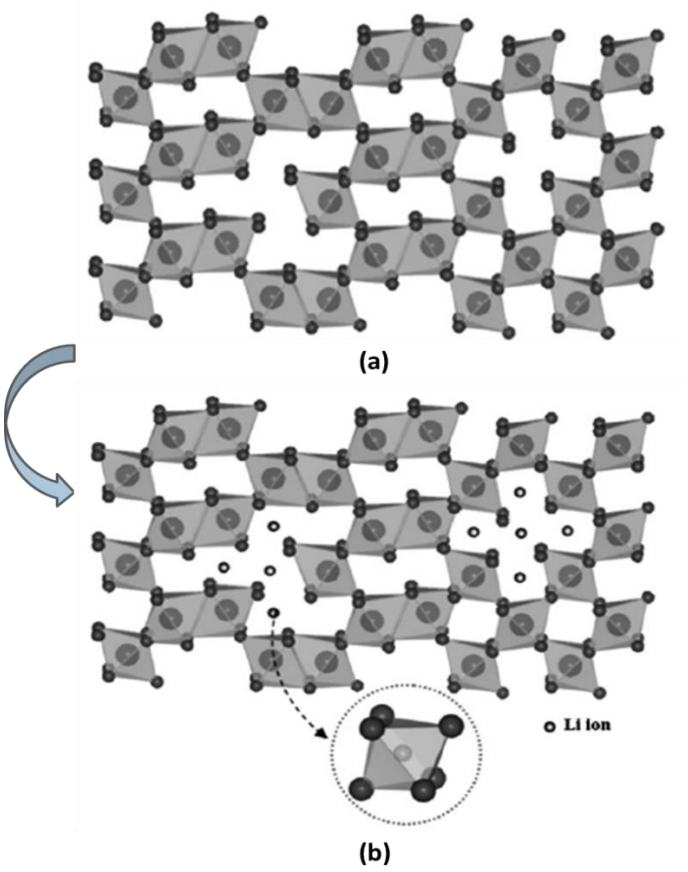

Figure 2.16. Schematic diagrams of: (a) untreated γ-MnO_2, (b) chemically lithiated γ-MnO_2 [86].

CHAPTER 3

EXPERIMENTAL

3.1. Materials

The γ-MnO_2 powder used as the sorbent material for lithium adsorption study, was purchased from China. Lithium chloride (LiCl) (anhydrous, analytical grade), was supplied from Loba Chemie (Mumbai, India), and used without further purification. For the desorption experiments, Hydrochloric Acid (HCl) ACS reagent 37% was supplied from ISOLAB (Wertheim, Germany). Sodium Hydroxide (NaOH) (pellets, puriss grade) was supplied by Sigma-Aldrich (St. Louis, MO, USA). For the preparation of buffer solutions, ammonia solution (%25 w/w) and NH_4Cl (ammonium chloride) powder of 99% purity were supplied from Merck (Darmstadt, Germany).

3.2. Equipment

3.2.1. Measurement of Li^+ concentration in aqueous solutions

The lithium-ion concentration in solutions was determined by the flame photometry method. The flame photometer works on the principle of measuring the amount of light emitted when a metal is inserted into a flame. Sheerwood 360 Flame photometer (Cambridge, UK) was used for the analysis. The device enabled the detection of lithium (Li^+), and four other cations (Na^+, Ba^{2+}, Ca^{2+}, K^+). Since the intensity of the flame's produced light is directly correlated with the concentration of the species being measured, the concentrations of desorbed Li^+ in solutions were initially determined by first creating a calibration curve using stock solutions with known concentrations of Li^+ ion.

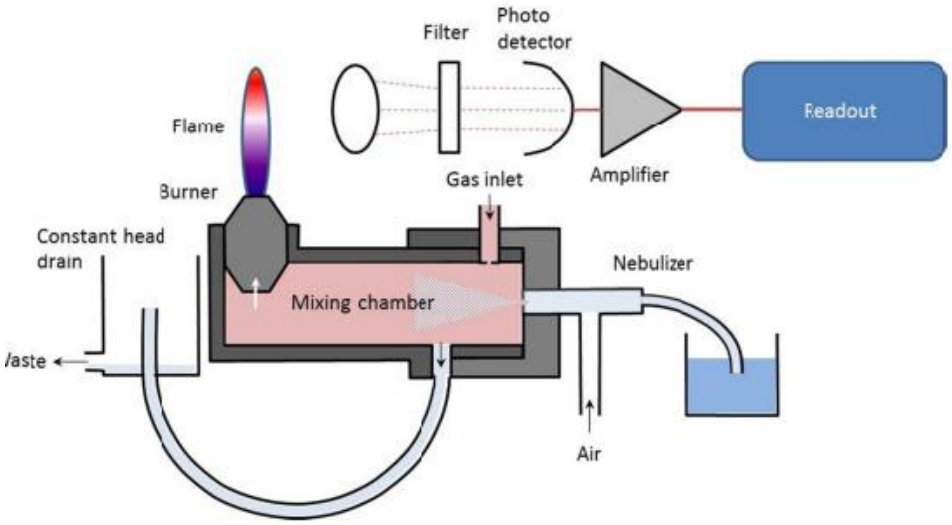

Figure 3.1. Schematic representation of a flame photometer [90].

The Inductively Coupled Plasma-Optical Emission Spectroscopy (ICP-OES) method was also used during the experiments for the determination of lithium-ion concentration in solutions. ICP-OES works on the principle of excitation of atoms when plasma energy is applied to the sample from the outside. As the excited atoms return to their lower energy states, the rays are emitted and those corresponding to the photon wavelength are measured. Finally, the type of element is determined by the position of the photon rays, while the content of these elements is determined by the intensity of the rays.[91]

3.2.2. Spectroscopic Methods

An X-ray diffractometer (XRD), the Philips X'Pert Pro (Eindhoven, Netherlands), was used to determine the crystalline structure of the sorbent powder and the phases it contains, with a copper anode as an X-ray source, a generator voltage of 45 kV, a tube current of 40 mA, and a Cu-Kα wavelength of 1.5406 Å. The sample was scanned between the 2θ angles of 10° - 80° and the scanning rate was 0.08° per second. The elemental composition of the sorbent was determined by using X-ray Fluorescence (XRF) spectrometry, SPECTRO IQ II (Kleve, Germany).

3.2.3. Particle Characterization

The specific surface area and porosity of the sorbent were analyzed using the Brunauer-Emmett-Teller (BET) surface area and porosimetry analyzer (ASAP 2020, Micromeritics Instruments, Atlanta, GA). Measurements were performed isothermally at 77.4 K by using N_2 adsorption. Before the measurements, samples were degassed at 150 °C for 3 h in a vacuum. Scanning Electron Microscopy (SEM), FEI Quanta 250 Feg (Oregon, USA), was used to analyze the morphology of the sorbent. For the particle size and zeta potential measurements, Malvern dynamic light scattering (DLS) Nano-ZS instrument (Worcestershire, UK) was used.

3.3. Batch Adsorption Experiments

Several batch adsorption experiments were performed to understand the adsorption mechanism of the absorbent material and to examine its adsorption capacity. Analytical study of the sorbent was carried out to optimize the adsorption process. For the batch adsorption experiments, synthetic Li^+ containing solutions with different concentrations was prepared by dissolving LiCl in deionized water. The mixture obtained after the adsorption experiment was taken and centrifuged at 6000 rpm for 30 minutes. The remaining solid was isolated from the decantate, after which the lithium-ion concentration in the decantate and in the initial solution before adsorption was measured by the ICP-OES method. Prior to ICP-OES analysis, the samples were acidified with %2 of HNO_3 (nitric acid). The parameters including, sorbent amount, adsorption time, initial Li^+ concentration, solution pH and temperature were investigated.

The adsorption capacity (mg/g) of the sorbent is calculated by Equation (3.1),

$$Q_t = \frac{(C_0 - C_t)\times V}{W} \tag{3.1}$$

Where C_0 is the initial Li^+ concentration in solution (mg/L); Ct is the Li^+ concentration of the solution after the adsorption process at time t (mg/L); V is the volume of solution (L); and W is the weight of the ion sieve (g).

3.3.1. Sample Preparation

Synthetic Li^+ solutions of known concentrations were prepared. To prepare 200 ppm lithium solution, 606.1 mg of LiCl was dissolved in 500 mL of deionized water. Other concentrations were prepared by diluting the 200 ppm stock solution. For example, for 100 ppm lithium solution, 50 mL of 200 ppm solution was taken and diluted with 1 to 2 ratio by adding up to 100 mL with deionized water.

For the preparation 1M of HCl, which was used for pH adjustment in the experiments, 41.6 mL of 37% HCl (12 M) was taken, first added to 250 mL deionized water in a 500 mL volumetric flask, and then completed with deionized water up to 500 mL. For the preparation of the buffer solutions, (prepared with 1 mol/L NH_3 and 1 mol/L NH_4Cl solutions). To prepare 1 M (NH_3) ammonia solution, 26 mL of 25% ammonia solution (13.4 M) was taken and made up to 350 mL with deionized water. For the preparation of 1M NH_4Cl solution, 13.4 g of NH_4Cl was weighed and dissolved in 200 mL of deionized water. The pH values of the buffer solution were adjusted using different molar ratios of NH_3/NH_4Cl.

3.3.2. Sorbent Amount and Initial Li^+ Concentration

To investigate the effect of the γ-MnO_2 amount on Li^+ adsorption performance; 30, 60, 90, 120 and 150 mg of γ-MnO_2 were added to 30 mL of 50 ppm Li^+ solution in a 50 mL beaker and stirred continuously at room temperature for 24 h.

In order to examine the effect of initial Li^+ concentration on the adsorption capacity of γ-MnO_2, 60 mg of γ-MnO_2 powder was weighted and added to 30 mL of LiCl solutions with Li^+ concentrations of 25, 50, 100 and 200 ppm and stirred continuously in a 50 mL beaker at room temperature for 24 h.

3.3.3. Solution pH

In order to study the effect of solution pH on lithium adsorption performance of γ-MnO_2, 60 mg of γ-MnO_2 was added into 30 mL of solution with different pH values of

6, 8, 10 and 12, and stirred continuously at room temperature for 24 h. The pH adjustments were done by using droplets of 2.0 M of NaOH and 1.0 M HCl solutions. Then, in order to keep the pH of the solution constant throughout the experiment, NH_4Cl-NH_3 buffer solutions were prepared for the pH range of 8-11. Afterwards, the same experimental procedure was applied for the adsorption mediums adjusted to different pH values with the buffer solution.

3.4. Adsorption Study in Tuzla Geothermal Power Plant

Adsorption study was carried out in real field. Tuzla geothermal power plant was selected as model field since Li^+ concentration is relatively higher compared to other plants in Turkey. Extracting valuable ions from a geothermal brine is a challenge because the translational velocity is high, the brine is salty. The system is hot meaning that the used material should resist and it contains lots of coexisting similar ions for instance Na^+ and Mg^{2+} which could interfere the selective extraction of lithium ion. Therefore, the γ-MnO_2 powder is placed in a reactor near the re-injection well. It is considered to be the best placement of the system energy harvesting is already done before the lithium uptake process. Textile filters are used, the sorbent powder is placed in. An adhesive epoxy resin is applied to the coverage of the filter to keep the sorbent powder in it, otherwise powder is removed from the textile filter via brine flow. The study was carried out at 87 °C and 2 bar conditions in the reinjection well system. Then, 1.5, 3.0, 17.0, 18.5, and 20 h of sorption times were employed as a process parameter. After the sorption study was completed, the sorbent material (γ-MnO_2 powder) treated with the geothermal brine was used in desorption experiments.

Figure 3.2. Photographic image of the mini-pilot system in Tuzla GPP at Ayvacık, Turkey

3.5. Desorption Experiments

A series of experiments were conducted to investigate the desorption behavior of Li^+ loaded γ-MnO_2 in diluted hydrochloric acid (1.0 M HCl). Certain amount of brine-treated sorbent powder is put into acidic solution. The idea is to replace Li^+ ions that is placed in the vacancies of the γ-MnO_2 structure with H^+ (protons). Then, the mixture obtained was taken and centrifuged at 6000 rpm for 30 min. The remaining solid was isolated from the decantate and the lithium-ion concentration in the decantate was measured by flame photometry method. For the flame photometry analysis, a blank and standard Li^+ solutions were prepared using lithium chloride (LiCl) and deionized water to construct a calibration curve with a concentration range containing the expected Li^+ concentrations. Thus, the intensity values recorded from the flame photometer fall somewhere within the range of the calibration curve. The parameters including the sorption time, sorbent amount, desorption time, solution pH, and repetitive desorption to enrich the Li^+ concentration were studied.

3.5.1. Sorption time

The γ-MnO_2 treated with brine at different sorption times of 1.5, 3.0, 17.0, 18.5, and 20 h was taken and 10 g of each were added to 30 mL of 1.0 M HCl in a beaker and stirred continuously at room temperature for 24 h. At the end of the experiment, the desorbed lithium concentrations in the solution were measured and compared to investigate the effect of the sorption time on Li^+ uptake performance.

3.5.2. Sorbent Amount

In this part of the experiment, in order to examine the effect of the Li^+ loaded γ-MnO_2 amount on Li^+ desorption performance; 0.5, 1.0, 1.5, 2, 2.5, 5.0, 7.5, and 10 g of Li^+ loaded γ-MnO_2 were added to 30 mL of 1M HCl and stirred continuously at room temperature for 24 h.

3.5.3. Desorption time

In the desorption time experiment, the desorption efficiency of lithium-ion was tested for different desorption times. 10 g of Li^+ loaded γ-MnO_2 was added into 30 mL of 1.0 M HCl and stirred continuously in a 100 mL beaker at room temperature for 3, 6, 9, 12, 24 and 48 h of desorption times.

3.5.4. Solution pH

The effect of the pH on lithium desorption efficiency of the desorbing agent was tested for 24-hours of desorption time. In this experiment, 10 g of Li^+ loaded γ-MnO_2 was added into 30 mL of solution with different pH values (2,4,6,8 and 10), and stirred continuously at room temperature. The pH adjustments were done by using 1.0 M of NaOH and HCl solutions.

3.5.5. Repetitive desorption

Repetitive desorption experiments were carried out to enrich the Li^+ concentration of the solution from low concentrations, as well as removing the other ions present in the geothermal brine. In this experiment, 10 g of brine-treated γ-MnO_2 powder was added to 30 mL of 1.0 M HCl in a 50 mL beaker and stirred for 24 h, centrifuged for 30 min at 6000 rpm to separate the decantate and the remaining solid. Then, the decantate was separated and 10 g of brine-treatedγ-MnO_2 was added into the decantate again. This process was repeated for 4 cycles (days) and at the end of each process, the Li^+ concentration in the decantate was measured.

3.5.6. Reuse of γ-MnO_2

Although the absorbent material is affordable (about $3/kg), the potential re-use of the material is of economic importance, especially given the need to use large quantities of sorbent material. Therefore, comparison of the adsorption performance between virgin sorbent and second use is examined in this study. To observe the reusability of the absorbent material, the remaining γ-MnO_2 solid after the desorption experiments was collected after centrifugation and used for re-use experiments. In the re-use experiments, the separated sorbent was again subjected to adsorption process in Tuzla geothermal brine for 15 h. Afterwards, the sorbent that is subjected to adsorption process for the second time, is subjected to a desorption experiment. In the desorption experiment, 0.3 g, 2 g and 10 g of the virgin and re-used γ-MnO_2 were added to 30 mL of 1.0 M HCl solution and stirred at room temperature for 24 h on a magnetic stirrer to compare their desorption results. Then, to investigate whether the desorption efficiency of reused γ-MnO_2 was affected by the desorption time, experiments were performed for 24 and 48 h.

CHAPTER 4

RESULTS AND DISCUSSION

4.1. Structural and Morphological Analysis of γ-MnO_2 powder

4.1.1. XRD and XRF of γ-MnO_2 sorbent

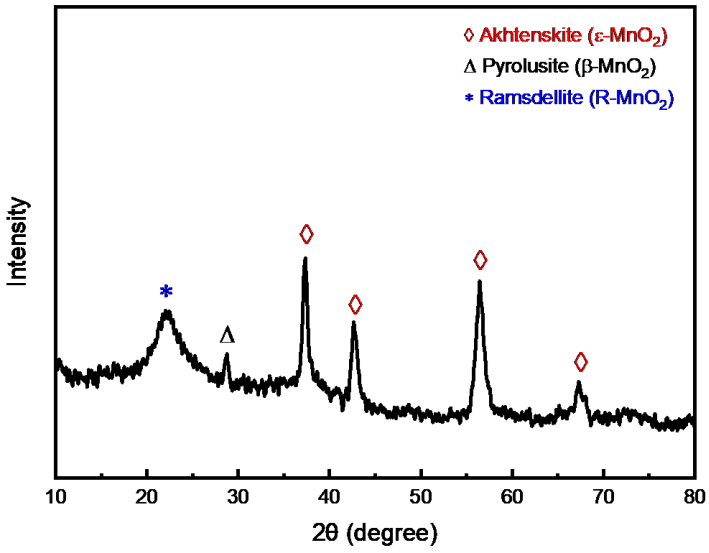

Figure 4.1. XRD pattern of the γ-MnO_2 powder

Figure 4.1 presents XRD pattern of γ-MnO_2 (EMD) powder purchased from China and provides the structural information. The XRD results show that the reflections can be indexed to a mixture of three phases: akhtenskite (ε-MnO_2), pyrolusite (β-MnO_2) and ramsdellite (R-MnO_2), which are different polymorphs of MnO_2. The broad reflection observed at the 2θ angle of 22.1° corresponds to the (001) plane of ramsdellite (R-MnO_2) phase and the peak 28.7° may likely from (110) plane of pyrolusite (β-MnO_2) polymorph. Pyrolusite (β-MnO_2), has a tetragonal structure and is the stable form of MnO_2 at ambient temperatures, whereas ramsdellite (R-MnO_2) has orthorhombic structure.[92] The diffraction peaks observed at an angle of 37.3°, 42.6°, 56.4° and 67.5° likely correspond to the akhtenskite (ε-MnO_2) phase with (100), (101),

(102) and (110) planes, respectively. Akhtenskite (ε-MnO_2) is a metastable polymorph of MnO_2 with hexagonal structure.[92] The multiphase XRD model of the γ-MnO_2 is in agreement with the study by Kim et al.[14], which observed ε-MnO_2 as an independent phase present in a conventional EMD material. The commercial EMD studied was found to be multiphase and contained R-MnO_2, ε-MnO_2 and β-MnO_2.

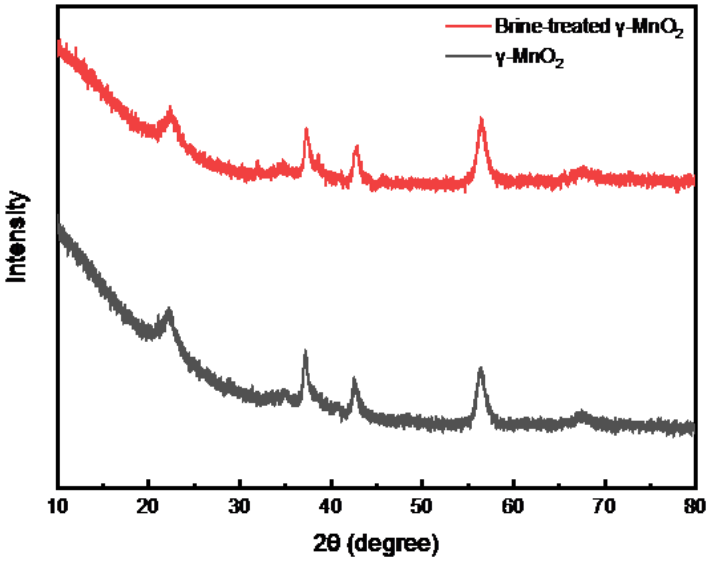

Figure 4.2. XRD patterns of the γ-MnO_2 before and after treated with geothermal brine

The XRD pattern of the γ-MnO_2 powder before and after treated with geothermal brine are shown in Figure 4.2. As the XRD patterns show, the permanent signals before and after treated with geothermal brine are similar to each other, which can be indicate that the structure is retained after the adsorption of lithium takes place. The reflections located at 2θ angle of 22.40°, 37.31°,42.74° and 56.47° for the sorbent before treated with brine and at 22.24°, 37.14° and 42.62° and 56.28° for the sorbent after the brine treatment. The lattice spacing (*d*) of the mentioned diffraction peaks were estimated as 3.97 Å, 2.41 Å, 2.12 Å and 1.63 Å for before and 4.00 Å, 2.42 Å, 2.12 Å and 1.64 Å for the sorbent after treated with brine.

Based on the 2θ values indicated, the XRD pattern of the sorbent after brine treatment shifted to a slightly lower angle compared to the sorbent in the first state, which could be due to lattice expansion. It can be attributed to the incorporation of certain ions found in salt water (e.g. Li^+ and Na^+) into the lattice structure.[93,94] This is also consistent with the increase in the *d* (lattice spacing) values.

Table 4.1. Elemental Composition of the γ-MnO_2 powder

Element	(w/w) %	Oxide	(w/w) %
Na	4.18	Na_2O	5.64
Mn	70.13	MnO	90.55

Table 4.1 gives the elemental composition of the commercial powder. As theoretically expected, the majority of the powder's content is Mn nearly 70% by mass. However, it was determined that there was approximately 4% Na in the structure. In addition, there are negligible amounts of impurities such as Mg, Al and Ca elements in the structure. Since XRF analysis gives the compounds both in oxide form and elemental composition, the MnO_2 content is a higher at %90.55 and Na_2O is 5.64%. The origin of the Na content in the γ-MnO_2 powder could be the Na additives used in the treatment during mining of MnO_2 ore.[95]

4.1.2. Zeta Potential of γ-MnO_2

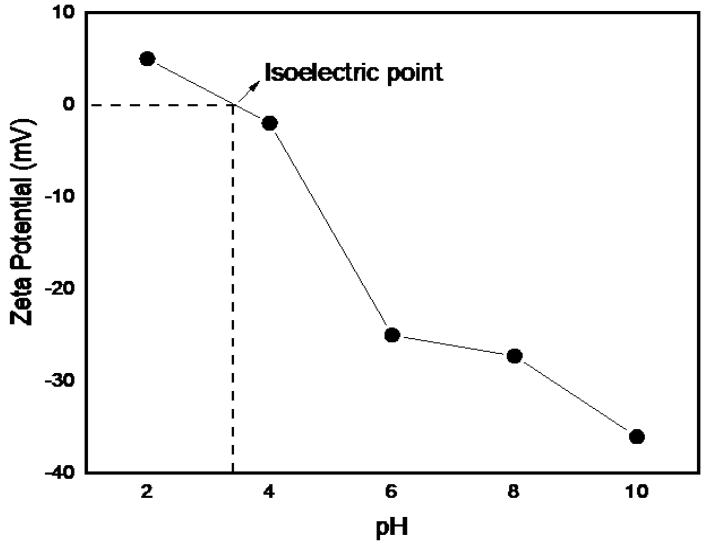

Figure 4.3. Zeta potential of γ-MnO_2 at different pH values.

To gain more insight into the factors affecting sorption at the tested pH values, zeta potential was measured for the sorbent at various pH values. For zeta potential measurements, 10 mg of γ-MnO_2 was dispersed in 100 mL of 1 mmol/L NaCl solution, the pH was adjusted to 2-10 with 0.1 M HCl and NaOH, and the suspension was allowed to settle for 24 h before measurement. Figure 4.3 shows the zeta potential

values varying in the pH range of 2-10. It was observed that as the pH increased, the charge negativity increased. The increase in the negative charge of the particles may have increased the attractive force between the positively charged lithium ion, thus achieving higher sorption efficiency. This result is in agreement with other studies. For example, Zhang et al[91] compared surface zeta potentials of the varied MnO_2 polymorphs including α-, β-, γ-, δ-, and λ-MnO_2 as a function of solution pH and observed that surface zeta potentials of all adsorbents decreased due to the continuous deprotonation effect of surface hydroxyl groups. The zero charge point (pH_{pzc}) of the γ-Mno_2 sorbent was determined as 2.8, which is consistent with the literature since manganese oxides, a type of surface acidic oxides, have zero charge point values between 2.0-4.5.[14]

4.1.3. Particle Size Distribution and BET Analysis of γ-MnO_2

The specific surface area, pore volume and average pore diameter of γ-MnO_2 powder were measured by The Brunauer-Emmett-Teller (BET) method using the nitrogen gas adsorption-desorption at 77 K. For γ-MnO_2, a specific surface area of 33.7 $m^2\ g^{-1}$, a total pore volume of 0.065 cm^3g^-1, and average pore diameter of 76.9 Å (7.69 nm) were obtained, indicating that the sorbent powder has a mesoporous structure.[96] The particle size distribution of γ-MnO_2 nanoparticles measured by the Dynamic Light Scattering (DLS) method is given in Figure 4.4. The average diameter particle size was observed as 50.89 nm.

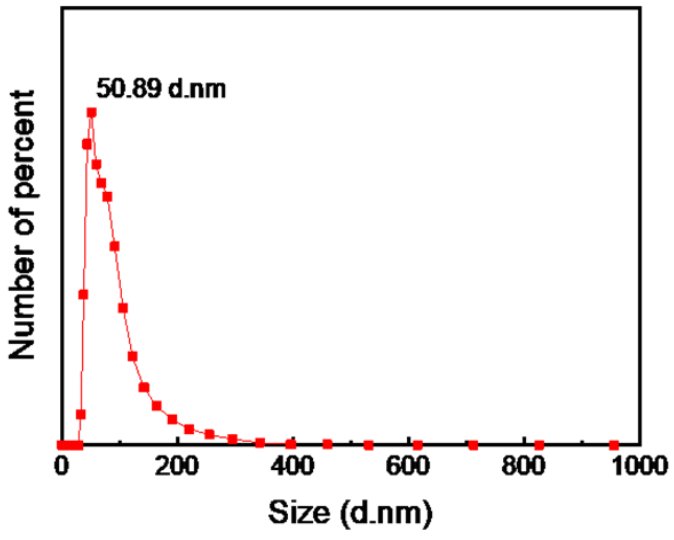

Figure 4.4. Particle size distribution of γ-MnO_2

4.1.4. SEM images of γ-MnO_2 powders

The morphology of the γ-MnO_2 powder was investigated by SEM using secondary electron detector. A serious aggregation is observed in the structure, which is not a surprise since the imaging is performed on solid powder samples. Submicron diameter spherical morphology is observed as the primary particles in aggregates. Any other phase regarding with nearly 4% by mass of Na was observed in the structure.

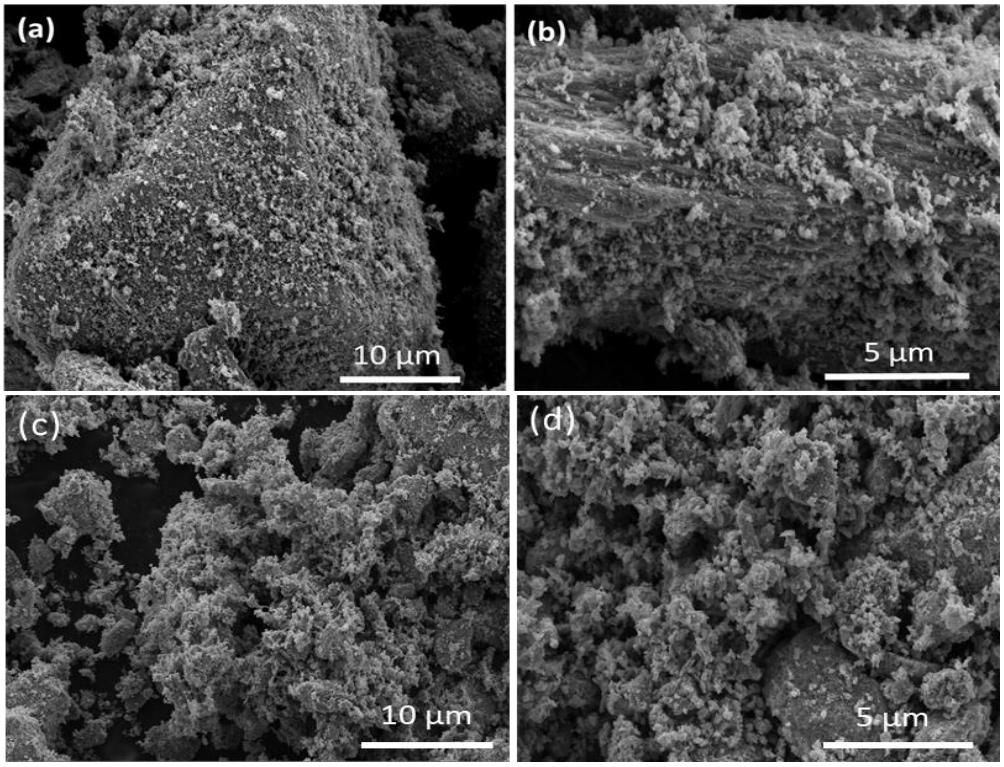

Figure 4.5. SEM images of the γ-MnO_2 powder at 10 000 × (a,c) and 25 000 × (b,d) magnification

4.1.5. Elemental Composition of Sorbent After the Sorption and Desorption Process

Table 4.2 presents elemental composition of γ-MnO_2 before and after the sorption as well as after desorption processes. It was observed that the amount of Na^+ in the sorbent increased after the sorption process. This is an expected result due to the

high Na^+ content of the geothermal brine. Upon interaction, most probably it leaves Na^+ on the surface of the structure. The same is true for all elements in the brine. Since a lot of elements adhered to the surface of the sorbent, the total weight and its composition is varied. For instance, Mn content seems to decrease. However, Mn content remains unchanged, total mass increased upon the adsorption of other elements like Na^+. After desorption, the values of the elements coming with the interaction with the brine decreases. However, the percent composition did not recover to the initial values. Some of the elements remained adhered to the surface of the sorbent.

Table 4.2. Elemental composition of γ-MnO_2 before/after the sorption and desorption process

Element	(%)		
	Before sorption	**After sorption**	**After desorption**
Na	4.2	8.90	6.0
Mn	70.1	60.1	66.3
Ca	0.10	1.63	0.10
Cl	0.005	1.24	1.0
Mg	1.0	1.27	1.1
Fe	0.003	1.28	0.8
Sr	0.008	0.53	0.1
Ba	0.03	0.40	0.4
Al	0.2	0.40	0.3

4.1.6. Morphological Analysis of the Sorbent Before and After the Sorption

The morphology of the ***γ***-MnO_2 before and after the brine treatment is investigated by using the scanning electron microscopy as given in Figure 4.6. No physical change was observed in ***γ***-MnO_2 before and after the sorption study. Since MnO_2 is a ceramic material, it is resistant against temperature and salinity of the brine.

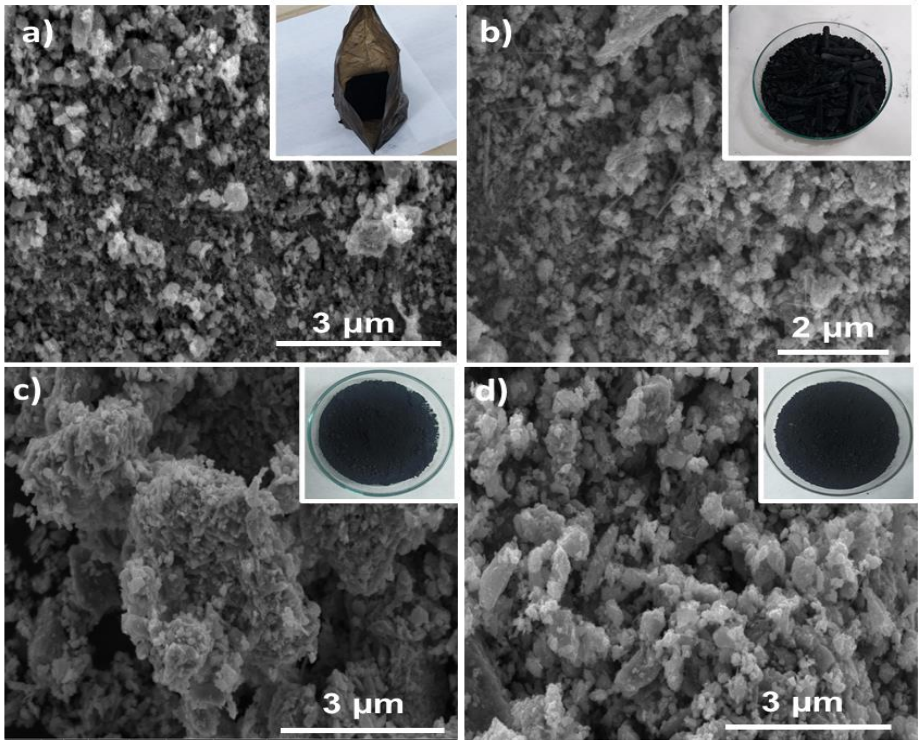

Figure 4.6. The morphology of the γ-MnO_2 powder before (a,c) and after treated with geothermal brine (b,d)

4.2. Batch Adsorption

4.2.1. Effect of Sorbent Amount on Adsorption Performance

The effect of the γ-MnO_2 dose on the adsorption performance is given in the Figure 4.7. According to the experimental results, the removal of Li^+ from solution was increased when the sorbent dose was increased from 2 g/L to 20 g/L. An increase in the surface area and the larger availability of active sites on the surface of γ-MnO_2 could be the origin of the increase in the Li^+ removal. However, as the sorbent amount increases, adsorption capacity was found to be decrease. This result can be explained by the aggregation of the sorbent when it increases above a certain amount, resulting in a decrease in the active surface area. Sorption capacity was found to be 6.2 mg/g when the sorbent concentration was 3 g/L. This value is a bit smaller than the values reported in the literature, which lies between 15-50 mg/g for various conditions.[97] Although this value seems smaller, the conditions and the scale of the adsorption process are different. The first difference is that the commercial sorbent material used can be ordered in tones

and supplied within days. This is not possible for lab-made MnO_2 materials. In addition, γ-MnO_2, whose electrochemical activity is normally studied for lithium-ion batteries, can be expected to show lower adsorption performance than conventional lithium manganese oxide ion-sieves.

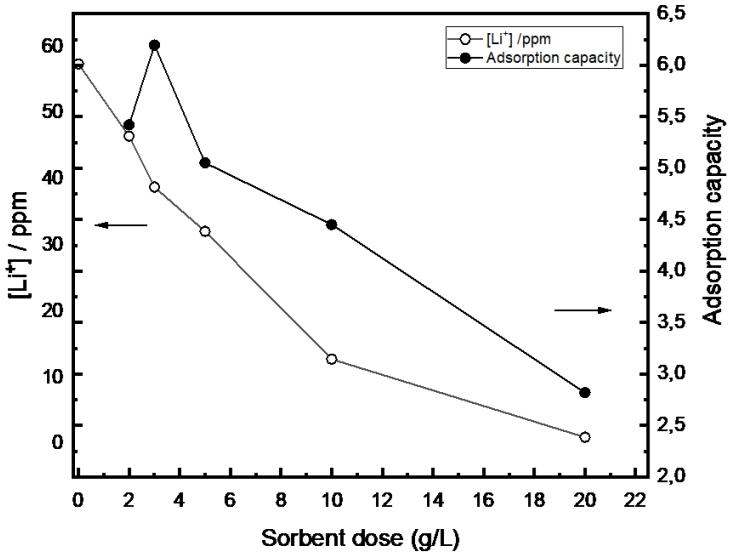

Figure 4.7. Sorbent amount in dispersion vs. Adsorption performance (C_0 =57 mg/L, pH=13, time 24 h, at RT.)

4.2.2. Effect of initial Li^+ Concentration of Solution

The variation of the adsorption capacity of γ-MnO_2 with respect to the initial Li^+ concentration of the solution is given in Figure 4.8. The adsorption capacity is found to increase as the Li^+ concentration of the solution in which the adsorption is performed increases. The capacity reaches the adsorption capacity of 6.4 mg/g when the concentration was 200 ppm. The sorption process is claimed to be governed by two steps, which are boundary layer diffusion and intraparticle diffusion. By increasing the initial concentration of Li^+, the surface of the adsorbent is contacted with more Li^+, which is resulted by the diffusion of the Li^+ at a larger amount through the boundary layer in unit time.[98] In other words, the surface of the adsorbent may not have been fully bound with the adsorbates at the beginning of the adsorption process, whereas at the optimum initial lithium concentration, all surfaces of the active site may have been filled with adsorbates.[99]

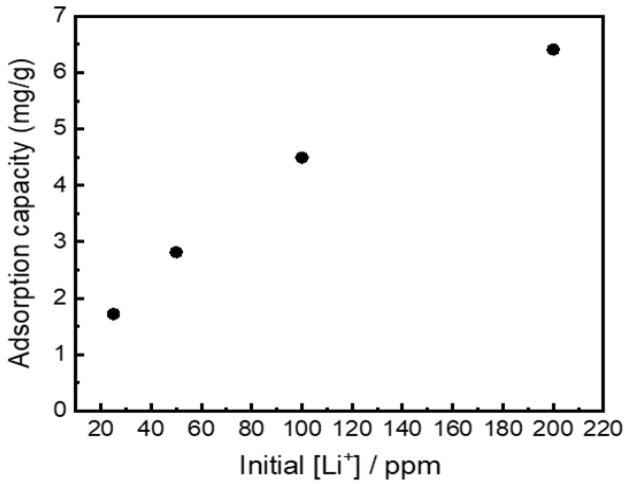

Figure 4.8. Initial Li^+ concentration in solution vs. Adsorption capacity (pH=12, sorbent dose of 2 g/L, at RT for 24 h)

4.2.3. Effect of pH on Adsorption Capacity

Figure 4.9. and 4.10. show the adsorption capacity at various pH of the solution. The adsorption capacity of the γ-MnO_2 powder show remarkable increase as the pH value of the Li^+ solution in which the adsorption process took place increased. The highest sorption capacity for γ-MnO_2 was achieved at pH 12 with a value of 1.8 mg/g. The uptake of lithium ions by the γ-MnO_2 sorbent was found higher under basic medium as the surface sites were more negatively charged at higher pH levels. As the electrostatic interaction between the positively charged Li^+ and the sorbent became stronger, the surface exhibited a larger affinity for adsorbing the Li^+.[45]

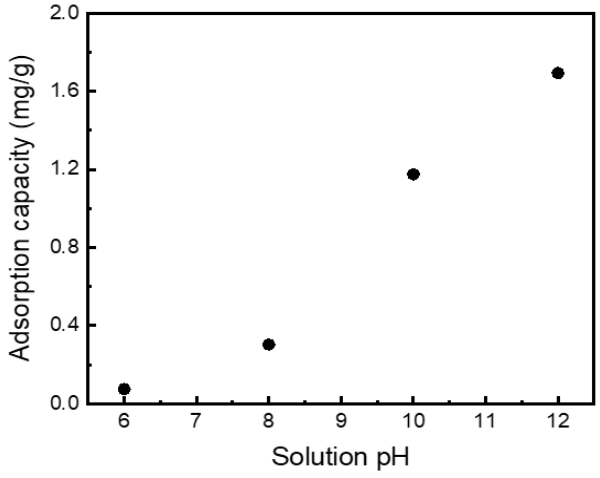

Figure 4.9. Solution pH vs. Adsorption capacity (sorbent dose of 2 g/L, at RT for 24 h)

This result is also compatible with studies in the literature on the effect of pH on adsorption capacity. Park et al[100] studied the change of lithium sorption capacity in the pH range of 2-10 and observed that the sorption capacity increased as the pH increased and reached the highest sorption capacity of 6-7 mg/g at pH 10. Another example from the literature, Yang et al[79] also studied lithium sorption of λ-MnO_2 in the pH range of 4-11 and observed that the adsorption capacity of λ-MnO_2 is very low under acidic condition. The adsorption capacity of λ-MnO_2 increased sharply as the pH increases, and reached a maximum at pH>10, indicating that the alkaline medium favored lithium sorption. The increase in the sorption amount is due to the deprotonation effect of the surface hydroxyl group with increasing pH, which is valid for manganese oxides, is interpreted in the same way for γ-MnO_2.

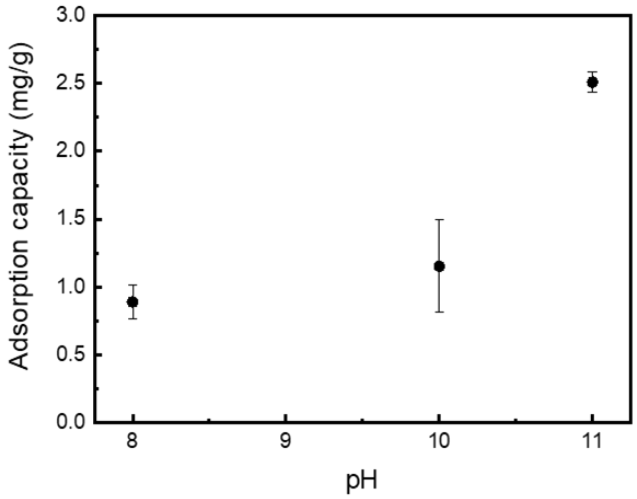

Figure 4.10. Solution pH vs. adsorption capacity when buffer solution is used (sorbent dose of 2 g/L, at RT for 24 h)

Figure 4.10 gives the result of the experiment using NH_4Cl-NH_3 buffer solution in order to keep the pH of the solution constant during the adsorption experiment. The adsorption capacity was found to be higher in the experiment using the buffer system compared to basic solution prepared by NaOH. The reason of this result may be the effect of Na^+ is prevented since Na^+ competes with Li^+.

4.2.4. Sorption Isotherms

In order to study the sorption isotherms of the γ-MnO_2 sorbent for lithium, 0.06 g of λ-MnO_2 powder was contacted with 30 mL of LiCl solutions with Li^+ concentrations ranging from 25 to 200 mg/L. Each sample was stirred continuously for 24 h at 18°C to obtain the final equilibrium Li^+ concentration. In order to fully understand the interaction between sorbate and sorbent and to make the most effective use of the sorbent, the fitting of the sorption isotherm models is essential. Models of the Langmuir and Freundlich isotherms were fitted to the experimental data of Li^+ adsorption by γ-MnO_2 sorbent as a function of equilibrium concentration. The results are shown in Figure 4.11 and 4.12, respectively, where the linearized forms of the Langmuir and Freundlich isotherm models are expressed by Eqs (4.1) and (4.2)[101]:

$$\frac{C_e}{q_e} = \frac{1}{q_m} C_e + \frac{1}{K_L q_m} \quad (4.1)$$

$$\log q_e = \frac{1}{n} \log C_e + \log K_F \quad (4.2)$$

Where Ce denotes the solution's equilibrium Li^+ concentration in mg L^{-1}, *qe* denotes the equilibrium Li^+ adsorption capacity in mg g^{-1}, *qm* denotes the theoretical maximum adsorption capacity in mg g^{-1}, and K_L denotes the Langmuir empirical constant in Lmg^{-1}. The slope and intercept of the plot of Ce/qe vs. Ce can be used to calculate the values of *qm* and K_L. The Freundlich constants K_F and n, measured in mg g^{-1} and g L^{-1} respectively, depend on temperature and system. The slope and intercept of the log qe vs. log Ce plot can also be used to determine the values of n and K_F.

The calculated isotherm parameters for Li^+ adsorption by γ-MnO_2 are listed in Table 4.3. The experimental data provided a better fit with the Langmuir isotherm rather than with the Freundlich isotherm, according to the correlation coefficients (R^2) of 0.994 and 0.991 respectively. According to the literature [102], the monolayer adsorption of Li^+ on the surface of the γ-MnO_2 sorbent can be well described by the Langmuir isotherm, which also stated that the sorption took place on an adsorbent that is structurally homogeneous. γ-MnO_2 showed the maximum Langmuir adsorption capacity (*qm*) of 9.737 mg g^{-1}. Also, the Freundlich constant, n, is higher than 1 (n >1), meaning that the adsorption process is favourable.[101]

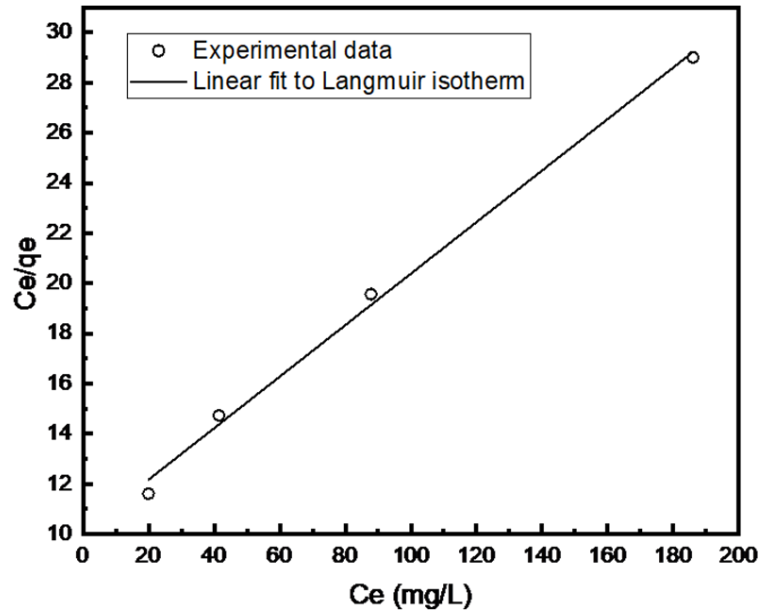

Figure 4.11. Langmuir Isotherm of Li^+ adsorption by γ-MnO_2

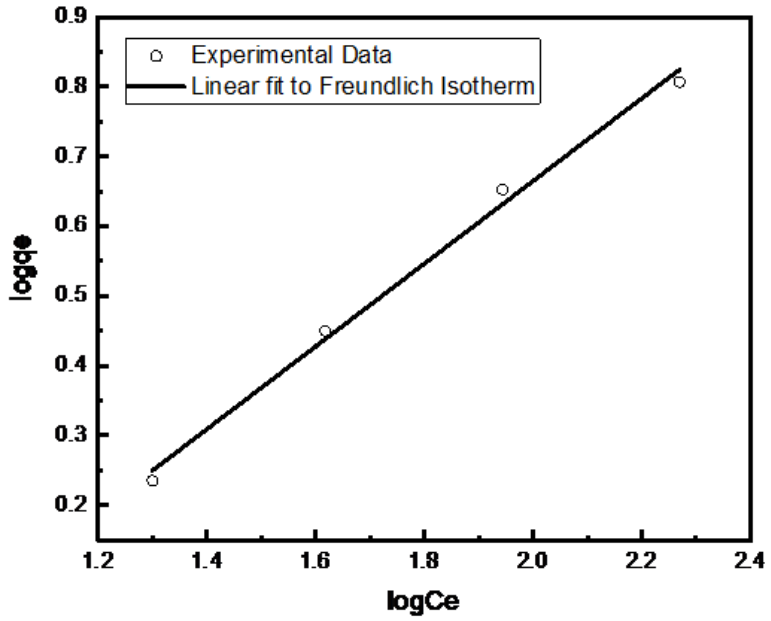

Figure 4.12. Freundlich Isotherm of Li^+ adsorption by γ-MnO_2

Table 4.3. Langmuir and Freundlich isotherm parameters

Langmuir isotherm			**Freundlich isotherm**		
qm (mg/g)	K_L / (L mg^{-1})	r^2	K_F / (mg g^{-1})	n /(g L^{-1})	r^2
9.737	0.010	0.994	0.301	1.686	0.991

4.3. Desorption

4.3.1. Effect of Sorption time on Desorption

Adsorption time is systematically investigated in the field from 1 to 24 h. The sorbent powder is put into acidic solution and lithium ion is released. The maximum concentration is achieved when the sorption time is shorter. As the adsorption time is extended, the concentration of the lithium released decreases. Figure 4.13. shows concentration of the lithium desorbed after various adsorption time. The brine-treated sorbent after the shorter sorption time released higher amount of lithium. Based on this result, one can conclude that the shorter sorption time better capacity is.

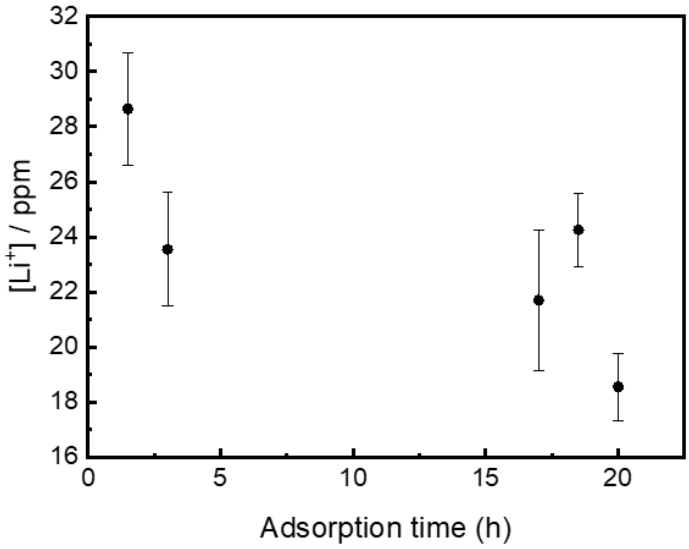

Figure 4.13. Sorption time in Tuzla GPP vs. Desorption performance (10 g of brine-treated γ-MnO_2 in 30 mL 1M HCl solution for 24h at RT)

4.3.2. Effect of Brine-treated Sorbent Amount

The concentration of Li^+ in decantate solution in the presence of various amount of γ-MnO_2 given in Figure 4.14. As the amount of sorbent increases, the amount of Li^+ released into the solution increased, and the concentration of Li^+ reached the maximum of approximately 26 ppm when 10 g of γ-MnO_2 was used. This is an expected result as the amount of lithium adsorbed sorbent increases, more lithium ions can be replaced with hydrogen atoms, resulting in more Li^+ ions being released into the acidic environment. Considering the highest desorbed Li^+ concentration obtained, 10 g was used as the sorbent amount in order to obtain the highest yield in the subsequent desorption parameter studies.

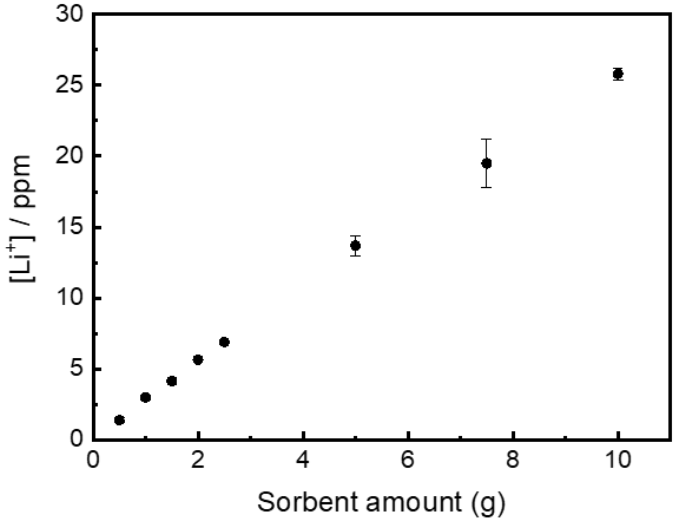

Figure 4.14. The concentration of Li^+ in decantate solution in the presence of various amount of γ-MnO_2. (Desorption in 30 mL 1M HCl solution for 24h at RT)

4.3.3. Effect of Desorption Time

According to the experimental results seen in Figure 4.15, the desorbed lithium concentration increased polynomially as the desorption time increased, although it did not significantly affect the desorption performance of lithium. At the end of the 3h of desorption period, the lithium concentration desorbed into the acidic environment was 18.5 ppm, while at the end of the 48h desorption period, the lithium concentration increased to a maximum of 27.5 ppm.

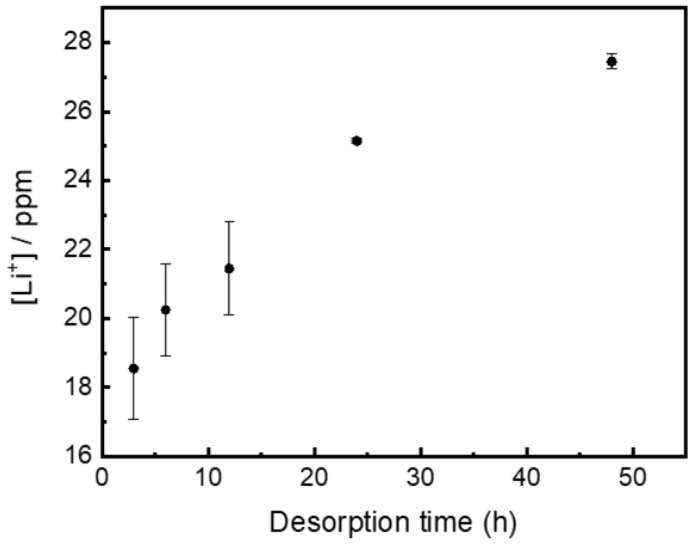

Figure 4.15. Li^+ concentration as a function of desorption time (10 g of brine-treated γ-MnO_2 in 30 mL 1M HCl solution at RT)

4.3.4. Effect of pH

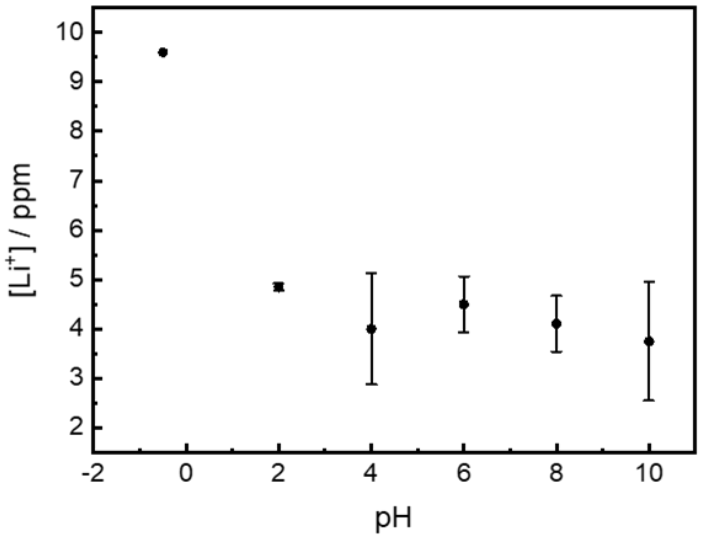

Figure 4.16**.** Li^+ concentration as a function of pH. (10 g of brine-treated γ-MnO_2 in 30 mL 1M HCl solution for 24h at RT)

The desorbed Li^+ concentration into solution with different pH values of the desorption environment given in Figure 4.16. When the pH of the desorption medium was between 2-10, the lithium concentration released to desorption environment ranged

between 3-5 ppm. When the pH was a highly acidic value of -1 (pH of 1M HCl solution), the lithium concentration in the desorption medium suddenly reached 19.6 ppm. The pH is a very decisive parameter for the desorption process since the desorption mechanism of Li^+ is due to the ion exchange with H^+ in solution. Therefore, a better desorption performance was observed as a result of more protons (more H^+) in the environment when the pH of the solution was lower.

4.3.5. Repetitive Desorption and Li^+ Enrichment

Repetitive desorption experiment was performed to enrich the Li^+ solution and the results given in Figure 4.17 at the end of the 4 days of repetitive desorption cycle. At the end of the 4th day, the Li^+ concentration is increased from 27 ppm to around 250 ppm. The higher the Li^+ concentration of the solution obtained after the desorption process, the easier it is to precipitate and extract lithium from the solution. This result is considerable in this respect. However, in order to precipitate the Li^+ ion in the form of $AlLiO_2$ or Li_2CO_3, the Li^+ concentration should be further enriched, perhaps by combining it with other methods. In the study of Zhu et al.[103], it was suggested that, increasing the lithium concentration enhanced the lithium recovery rate considerably, especially when the lithium concentration was in the 5–20 g/L range.

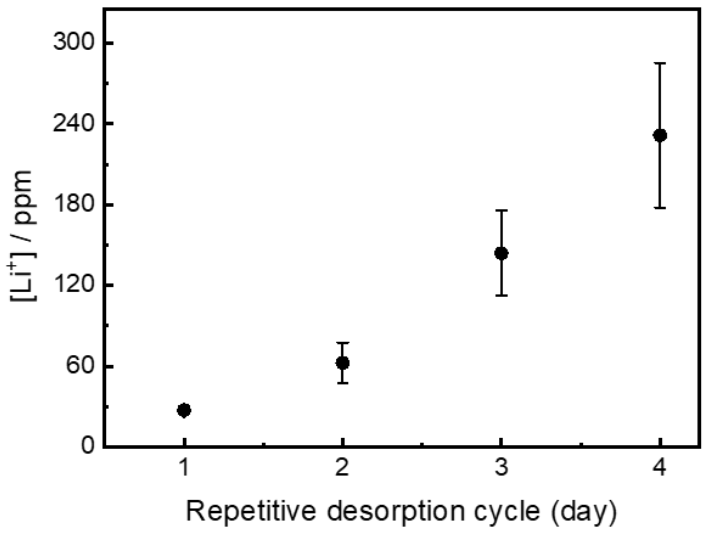

Figure 4.17. The concentration of Li^+ after repetitive desorption with powder treated with brine

4.3.6. Re-use of γ-MnO_2

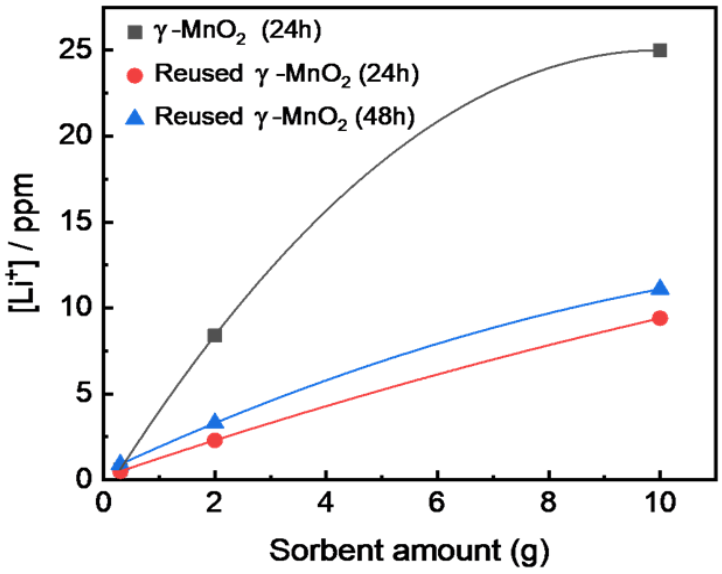

Figure 4.18. Re-use performance of the sorbent (Desorption in 30 mL 1M HCl solution at RT)

The reusability of the γ-MnO_2 absorbent material is worth considering from an economic point of view. The performance of the γ-MnO_2 powder is examined after desorption in acidic solution. As stated above, γ-MnO_2 contains vacancies in the crystal structure which is assumed to be filled with Li^+. The desorption process makes these vacancies empty again by releasing the lithium back out, and the remaining vacancies may be suitable for the second round of adsorption. After desorption, the powder is subjected to the adsorption process again in order to see how successfully the lithium is separated from the voids in the structure of the sorbent, and as a result, to understand its effectiveness in a second adsorption process. Figure 4.18. shows the Li^+ concentration after desorption of the powder of second use. The concentration was 9.4 ppm after 24 h desorption although the fresh powder yields 25 ppm. It shows slight increase to 11.1 ppm when the desorption time is extended to 48 h. Thus, the reuse of the powder shows almost 40% performance compared to virgin powder under the conditions employed.

CHAPTER 5

CONCLUSION

In this thesis, as a new approach, relatively inexpensive electrolytic manganese dioxide (γ-MnO_2), which is normally used as the cathode material in lithium-ion batteries, was used as an absorbent for the isolation of lithium from geothermal brine of Tuzla Geothermal Power Plant (TGPP). A mini-pilot system was installed in the reactor near the plant's reinjection well, using commercial electrolytic γ-MnO_2 for the adsorption process. In the first stage of the thesis, the characterization of γ-MnO_2 powder was carried out using XRD, XRF, SEM, BET and DLS methods and the compatibility of the powder used with commercial γ-MnO_2 was investigated. The XRD results show that the reflections of electrolytic γ-MnO_2 can be indexed to a mixture of three phases; β-MnO_2, ε-MnO_2 and R-MnO_2 as expected. Similar reflections obtained before and after treatment with geothermal brine were interpreted as the intercalation of lithium ion into the γ-MnO_2 structure without destabilizing the structure. By applying the (BET) method for γ-MnO_2, a mesoporous structure with a specific surface area of 33.7 $m^2\ g^{-1}$, a total pore volume of 0.065 $cm^3 g^{-1}$ and an average pore diameter of 76.9 Å (7.69 nm) was observed.

In the second part of the studies, solution pH, initial lithium concentration, and sorbent amount were studied in synthetic solution to examine the adsorption performance of the γ-MnO_2 sorbent. The effect of sorbent concentration on the adsorption capacity of γ-MnO_2 was investigated in the range of 2-20 g/L and it was observed that the maximum adsorption capacity of 6.2 mg/g was reached when the sorbent concentration was 3 g/L, but when the adsorbent concentration increased further, the lithium adsorption capacity was decreased due to the reduction in the active sites of the sorbent surface as a result of the agglomeration. In the pH study, the adsorption capacity of the γ-MnO_2 sorbent increased with increasing pH as a result of the deprotonation of the surface hydroxyl groups, and the maximum adsorption capacity was obtained at pH 12. At the optimum 200 mg/L of initial lithium concentration, the maximum adsorption capacity of 6.4 mg/g was reached, which is thought to be due to

the fact that all surfaces of the active site are filled with adsorbates. The Langmuir and Freundlich equilibrium models of lithium adsorption were investigated and it was found that the Langmuir model best describes the adsorption equilibrium showing monolayer adsorption. The maximum Langmuir adsorption capacity (q_m) of the γ-MnO_2 adsorbent was determined as 9.74 mg/g.

In the last part of the study, adsorption was carried out at 87 °C and 2 bar in Tuzla Geothermal Power Plant and then the absorbent powder treated with geothermal brine is subjected to desorption process under acidic medium. Lithium ions are obtained in the acidic solution at 25 ppm when the amount of γ-MnO_2 was 10 g. The maximum adsorption performance was achieved at 1 h of adsorption in the field showing that the shorter adsorption time is favorable. Repetitive desorption experiments were carried out to enrich the lithium concentration of the solution from low concentrations, as well as removing the other ions present in the geothermal brine. Lithium concentration was enriched to more than 250 ppm after four cycles of desorption. This level of concentration can be even further enriched when the number of cycles is increased. As an example, the solubility of Li_2CO_3 is 1 g/L meaning that this enrichment of lithium in repetitive desorption may be extended to the precipitation level. Although the γ-MnO_2 powder is affordable (about $3/kg), the potential reuse of sorbent is of economic importance, especially given the need to use large quantities of sorbent. Therefore, reusability studies were carried out and 40% performance was observed for the reused sorbent compared to the virgin sorbent.

As a result of the studies, the use of electrolytic γ-MnO_2 sorbent for lithium adsorption was found as a promising candidate for practical use in the separation of lithium from geothermal brines as a new approach. In the next step of the studies, the structure of the γ-MnO_2 powder can be improved and stabilized to increase the lithium adsorption capacity and increase the reusability of the sorbent. Thus, greater amounts of lithium ions can be recovered from high volume geothermal brine.

REFERENCES

(1) Xu, P.; Hong, J.; Qian, X.; Xu, Z.; Xia, H.; Tao, X.; Xu, Z.; Ni, Q. Q. Materials for Lithium Recovery from Salt Lake Brine. *J. Mater. Sci.* **2021**, *56* (1), 16–63.

(2) Butt, F. S.; Lewis, A.; Chen, T.; Mazlan, N. A.; Wei, X.; Hayer, J.; Chen, S.; Han, J.; Yang, Y.; Yang, S.; Huang, Y. Lithium Harvesting from the Most Abundant Primary and Secondary Sources: A Comparative Study on Conventional and Membrane Technologies. *Membranes (Basel).* **2022**, *12* (4), 373.

(3) Vikström, H.; Davidsson, S.; Höök, M. Lithium Availability and Future Production Outlooks. *Appl. Energy* **2013**, *110*, 252–266.

(4) Meshram, P.; Pandey, B. D.; Mankhand, T. R. Extraction of Lithium from Primary and Secondary Sources by Pre-Treatment, Leaching and Separation: A Comprehensive Review. *Hydrometallurgy* **2014**, *150*, 192–208.

(5) Lin, H.; Yu, X.; Li, M.; Duo, J.; Guo, Y.; Deng, T. Synthesis of Polyporous Ion-Sieve and Its Application for Selective Recovery of Lithium from Geothermal Water. *ACS Appl. Mater. Interfaces* **2019**, *11* (29), 26364–26372.

(6) Kavanagh, L.; Keohane, J.; Cabellos, G. G.; Lloyd, A.; Cleary, J. Global Lithium Sources-Industrial Use and Future in the Electric Vehicle Industry: A Review. *Resources* **2018**, *7* (3).

(7) Murodjon, S.; Yu, X.; Li, M.; Duo, J.; Deng, T. Lithium Recovery from Brines Including Seawater, Salt Lake Brine, Underground Water and Geothermal Water. *Thermodyn. Energy Eng.* **2020**, No. February 2021.

(8) Zhang, Y.; Sun, W.; Xu, R.; Wang, L.; Tang, H. Lithium Extraction from Water Lithium Resources through Green Electrochemical-Battery Approaches: A

Comprehensive Review. *J. Clean. Prod.* **2021**, *285* (xxxx), 124905.

(9) Ventura, S.; Bhamidi, S.; Hornbostel, M.; Nagar, A. Selective Recovery of Lithium from Geothermal Brines. **2020**, No. March, CEC-500-2020-020.

(10) Meng, F.; McNeice, J.; Zadeh, S. S.; Ghahreman, A. Review of Lithium Production and Recovery from Minerals, Brines, and Lithium-Ion Batteries. *Miner. Process. Extr. Metall. Rev.* **2021**, *42* (2), 123–141.

(11) Stringfellow, W. T.; Dobson, P. F. Technology for the Recovery of Lithium from Geothermal Brines. *Energies* **2021**, *14* (20).

(12) Zhang, Q. H.; Sun, S.; Li, S.; Jiang, H.; Yu, J. G. Adsorption of Lithium Ions on Novel Nanocrystal MnO2. *Chem. Eng. Sci.* **2007**, *62* (18–20), 4869–4874.

(13) Li, L.; Qu, W.; Liu, F.; Zhao, T.; Zhang, X.; Chen, R.; Wu, F. Surface Modification of Spinel λ-MnO 2 and Its Lithium Adsorption Properties from Spent Lithium Ion Batteries. *Appl. Surf. Sci.* **2014**, *315* (1), 59–65.

(14) Shin, J.; Seo, J. K.; Yaylian, R.; Huang, A.; Meng, Y. S. A Review on Mechanistic Understanding of MnO2 in Aqueous Electrolyte for Electrical Energy Storage Systems. *Int. Mater. Rev.* **2020**, *65* (6), 356–387.

(15) Gil-Alana, L. A.; Monge, M. Lithium: Production and Estimated Consumption. Evidence of Persistence. *Resour. Policy* **2019**, *60* (October 2017), 198–202.

(16) Pramanik, B. K.; Asif, M. B.; Roychand, R.; Shu, L.; Jegatheesan, V.; Bhuiyan, M.; Hai, F. I. Lithium Recovery from Salt-Lake Brine: Impact of Competing Cations, Pretreatment and Preconcentration. *Chemosphere* **2020**, *260*, 127623.

(17) Battistel, A.; Palagonia, M. S.; Brogioli, D.; La Mantia, F.; Trócoli, R. Electrochemical Methods for Lithium Recovery: A Comprehensive and Critical Review. *Adv. Mater.* **2020**, *32* (23).

(18) EVs to account for 79pc of lithium demand by 2030 | Argus Media https://www.argusmedia.com/en/news/2136196-evs-to-account-for-79pc-of-lithium-demand-by-2030 (accessed May 31, 2022).

(19) BMO Capital Markets https://capitalmarkets.bmo.com/en/ (accessed May 31, 2022).

(20) Survey, U. S. G. *Mineral Commodity Summaries 2020*; 2020.

(21) Sun, Y.; Wang, Q.; Wang, Y.; Yun, R.; Xiang, X. Recent Advances in Magnesium/Lithium Separation and Lithium Extraction Technologies from Salt Lake Brine. *Sep. Purif. Technol.* **2021**, *256* (August 2020), 117807.

(22) Swain, B. Recovery and Recycling of Lithium: A Review. *Sep. Purif. Technol.* **2017**, *172*, 388–403.

(23) Choubey, P. K.; Kim, M.; Srivastava, R. R.; Lee, J.; Lee, J. Advance Review on the Exploitation of the Prominent Energy-Storage Element : Lithium . Part I : From Mineral and Brine Resources. *Miner. Eng.* **2016**, *89*, 119–137.

(24) Lin, X.; Pan, F.; Wang, H. Progress of Li4Ti5O12 Anode Material for Lithium Ion Batteries. *Mater. Technol.* **2014**, *29* (A2), A82–A87.

(25) Sole, K. C.; Parker, J.; Cole, P. M.; Mooiman, M. B. Flowsheet Options for Cobalt Recovery in African Copper–Cobalt Hydrometallurgy Circuits. *Miner. Process. Extr. Metall. Rev.* **2019**, *40* (3), 194–206.

(26) Me, G. V.; Ayres, R. U. Lithium: Sources, Production, Uses, and Recovery Outlook ´ , 1. **2013**, *65* (8).

(27) Hannan, M. A.; Hoque, M. M.; Hussain, A.; Yusof, Y.; Ker, P. J. State-of-the-Art and Energy Management System of Lithium-Ion Batteries in Electric Vehicle Applications: Issues and Recommendations. *IEEE Access* **2018**, *6*, 19362–19378.

(28) Choubey, P. K.; Kim, M. S.; Srivastava, R. R.; Lee, J. C.; Lee, J. Y. Advance Review on the Exploitation of the Prominent Energy-Storage Element: Lithium. Part I: From Mineral and Brine Resources. *Miner. Eng.* **2016**, *89*, 119–137.

(29) Martin, G.; Rentsch, L.; Höck, M.; Bertau, M. Lithium Market Research – Global Supply, Future Demand and Price Development. *Energy Storage Mater.* **2017**, *6* (August 2016), 171–179.

(30) Lithium, G. Part 1 Lithium. **1993**.

(31) Chagnes, A.; Swiatowska, J. *Lithium Process Chemistry: Resources, Extraction, Batteries, and Recycling*; 2015.

(32) Chaves, C.; Pereira, E.; Ferreira, P.; Guerner Dias, A. Concerns about Lithium Extraction: A Review and Application for Portugal☆. *Extr. Ind. Soc.* **2021**, *8* (3).

(33) Starke, E. A.; Sanders, T. H.; Palmer, I. G. New Approaches to Alloy Development in the Al-Li System. *JOM J. Miner. Met. Mater. Soc.* **1981**, *33* (8), 24–33.

(34) Li, X.; Mo, Y.; Qing, W.; Shao, S.; Tang, C. Y.; Li, J. Membrane-Based Technologies for Lithium Recovery from Water Lithium Resources: A Review. *J. Memb. Sci.* **2019**, *591* (July), 117317.

(35) Point, M.; Point, B. Definitions, Mineralogy and Deposits. **2016**, No. June.

(36) Li, H.; Eksteen, J.; Kuang, G. Hydrometallurgy Recovery of Lithium from Mineral Resources : State-of-the-Art and Perspectives – A Review. *Hydrometallurgy* **2019**, *189* (June), 105129.

(37) Tadesse, B.; Makuei, F.; Albijanic, B.; Dyer, L. The Beneficiation of Lithium Minerals from Hard Rock Ores: A Review. *Miner. Eng.* **2019**, *131* (November 2018), 170–184.

(38) Choubey, P. K.; Kim, M.; Srivastava, R. R.; Lee, J.; Lee, J. Advance Review on the Exploitation of the Prominent Energy-Storage Element : Lithium . Part I : From Mineral and Brine Resources. *Miner. Eng.* **2016**, *89*, 119–137.

(39) Grosjean, C.; Herrera Miranda, P.; Perrin, M.; Poggi, P. Assessment of World Lithium Resources and Consequences of Their Geographic Distribution on the Expected Development of the Electric Vehicle Industry. *Renew. Sustain. Energy Rev.* **2012**, *16* (3), 1735–1744.

(40) Shahmansouri, A.; Min, J.; Jin, L.; Bellona, C. Feasibility of Extracting Valuable Minerals from Desalination Concentrate: A Comprehensive Literature Review. *J. Clean. Prod.* **2015**, *100*, 4–16.

(41) Siekierka, A.; Tomaszewska, B.; Bryjak, M. Lithium Capturing from Geothermal Water by Hybrid Capacitive Deionization G RA P H I C A L AB S T R A C T. **2020**, *436* (October 2017), 8–14.

(42) Li, L.; Deshmane, V. G.; Paranthaman, M. P.; Bhave, R.; Moyer, B. A.; Harrison, S. Lithium Recovery from Aqueous Resources and Batteries: A Brief Review. *Johnson Matthey Technol. Rev.* **2018**, *62* (2), 161–176.

(43) Xiang, W.; Liang, S.; Zhou, Z.; Qin, W.; Fei, W. Extraction of Lithium from Salt Lake Brine Containing Borate Anion and High Concentration of Magnesium. *Hydrometallurgy* **2016**, *166*, 9–15.

(44) The new “gold rush” for green lithium - BBC Future https://www.bbc.com/future/article/20201124-how-geothermal-lithium-could-revolutionise-green-energy (accessed Jun 30, 2022).

(45) Paranthaman, M. P.; Li, L.; Luo, J.; Hoke, T.; Ucar, H.; Moyer, B. A.; Harrison, S. Recovery of Lithium from Geothermal Brine with Lithium-Aluminum Layered Double Hydroxide Chloride Sorbents. *Environ. Sci. Technol.* **2017**, *51* (22), 13481–13486.

(46) Can, M. F.; Başaran, C.; Yildiz, A.; Demirkapi, M. Lithium Extraction from Geothermal Waters; a Case Study of Ömer-Gecek (Afyonkarahisar) Geothermal Area. *Turkish J. Earth Sci.* **2021**, *30* (SI-2), 1208–1220.

(47) Ilgar, R. Economic Contributions and Environmental Effects of Geothermal Energy: Çanakkale-Tuzla Geothermal Example. *Int. J. Res. Geogr.* **2019**, *5* (1), 1–8.

(48) Topcu, G.; Koç, G. A.; Baba, A.; Demir, M. M. The Injection of CO 2 to Hypersaline Geothermal Brine: A Case Study for Tuzla Region. *Geothermics* **2019**, *80* (January), 86–91.

(49) Baba, A.; Chandrasekharam, D. Geothermal Resources for Sustainable Development: A Case Study. **2022**.

(50) Zhang, Y.; Hu, Y.; Wang, L.; Sun, W. Systematic Review of Lithium Extraction from Salt-Lake Brines via Precipitation Approaches. *Miner. Eng.* **2019**, *139* (June), 105868.

(51) Zhao, X.; Jiao, Y.; Xue, P.; Feng, M.; Wang, Y.; Sha, Z. Efficient Lithium Extraction from Brine Using a Three-Dimensional Nanostructured Hybrid Inorganic-Gel Framework Electrode. *ACS Sustain. Chem. Eng.* **2020**, *8* (12), 4827–4837.

(52) Dahman, Y. Nanopolymers**By Yaser Dahman, Kevin Deonanan, Timothy Dontsos, and Andrew Iammatteo. *Nanotechnol. Funct. Mater. Eng.* **2017**, 121–144.

(53) Ola, P. D.; Matsumoto, M. Metal Extraction with Ionic Liquids-Based Aqueous Two-Phase System. *Recent Adv. Ion. Liq.* **2018**.

(54) Extraction Methods - Solution Pharmacy https://solutionpharmacy.in/extraction-methods/ (accessed Jun 10, 2022).

(55) Liu, G.; Zhao, Z.; Ghahreman, A. Novel Approaches for Lithium Extraction from Salt-Lake Brines: A Review. *Hydrometallurgy* **2019**, *187* (January), 81–100.

(56) Shi, D.; Cui, B.; Li, L.; Peng, X.; Zhang, L.; Zhang, Y. Lithium Extraction from Low-Grade Salt Lake Brine with Ultrahigh Mg/Li Ratio Using TBP – Kerosene – FeCl3 System. *Sep. Purif. Technol.* **2019**, *211* (September 2018), 303–309.

(57) Ji, L.; Hu, Y.; Li, L.; Shi, D.; Li, J.; Nie, F.; Song, F.; Zeng, Z.; Sun, W.; Liu, Z. Lithium Extraction with a Synergistic System of Dioctyl Phthalate and Tributyl Phosphate in Kerosene and FeCl3. *Hydrometallurgy* **2016**, *162*, 71–78.

(58) Li, H. fang; Li, L. juan; Li, W. Study of Lithium Extraction Mechanism by TBP Extraction System. *Chem. Phys. Lett.* **2022**, *791* (January).

(59) Zhou, Z.; Qin, W.; Liu, Y.; Fei, W. Extraction Equilibria of Lithium with Tributyl Phosphate in Kerosene and FeCl 3. *J. Chem. Eng. Data* **2012**, *57* (1), 82–86.

(60) Job, R. 1. Introduction. *Electrochem. Energy Storage* **2020**, 1–8.

(61) Shi, C.; Jing, Y.; Xiao, J.; Wang, X.; Yao, Y.; Jia, Y. Solvent Extraction of Lithium from Aqueous Solution Using Non-Fluorinated Functionalized Ionic Liquids as Extraction Agents. *Sep. Purif. Technol.* **2017**, *172*, 473–479.

(62) Dąbrowski, A.; Hubicki, Z.; Podkościelny, P.; Robens, E. Selective Removal of the Heavy Metal Ions from Waters and Industrial Wastewaters by Ion-Exchange Method. *Chemosphere* **2004**, *56* (2), 91–106.

(63) Chakraborty, R.; Asthana, A.; Singh, A. K.; Jain, B.; Susan, A. B. H. Adsorption of Heavy Metal Ions by Various Low-Cost Adsorbents: A Review. *Int. J. Environ. Anal. Chem.* **2022**, *102* (2), 342–379.

(64) Nageeb, M. Adsorption Technique for the Removal of Organic Pollutants from Water and Wastewater. *Org. Pollut. - Monit. Risk Treat.* **2013**.

(65) El-Baz, A.; Hendy, I.; Dohdoh, A.; Srour, M. Adsorption Technique for Pollutants Removal; Current New Trends and Future Challenges – A Review. *Egypt. J. Eng. Sci. Technol.* **2020**, *32* (1), 1–24.

(66) Patel, H. Fixed-Bed Column Adsorption Study: A Comprehensive Review. *Appl. Water Sci.* **2019**, *9* (3), 1–17.

(67) Girish, C. R.; Murty, V. R. Mass Transfer Studies on Adsorption of Phenol from Wastewater Using Lantana Camara, Forest Waste. *Int. J. Chem. Eng.* **2016**, *2016*.

(68) A, E. M.; Musin, E. Adsorption Modeling. **2001**, No. June, 577–708.

(69) Weng, D.; Duan, H.; Hou, Y.; Huo, J.; Chen, L.; Zhang, F.; Wang, J. Introduction of Manganese Based Lithium-Ion Sieve-A Review. *Prog. Nat. Sci. Mater. Int.* **2020**, *30* (2), 139–152.

(70) Julien, C. M.; Mauger, A. Nanostructured MnO2 as Electrode Materials for Energy Storage. *Nanomaterials* **2017**, *7* (11).

(71) Liu, L.; Zhang, H.; Zhang, Y.; Cao, D.; Zhao, X. Lithium Extraction from Seawater by Manganese Oxide Ion Sieve MnO2·0.5H2O. *Colloids Surfaces A Physicochem. Eng. Asp.* **2015**, *468*, 280–284.

(72) Zou, W.; Zhang, J.; Li, K.; Han, P.; Han, R. Characterization of Manganese Oxide and the Adsorption of Copper(II) and Lead(II) Ions from Aqueous Solutions. *Adsorpt. Sci. Technol.* **2009**, *27* (6), 549–565.

(73) Julien, C. M.; Massot, M.; Poinsignon, C. Lattice Vibrations of Manganese Oxides: Part I. Periodic Structures. *Spectrochim. Acta - Part A Mol. Biomol. Spectrosc.* **2004**, *60* (3), 689–700.

(74) Ooi, K.; Miyai, Y.; Katoh, S. Lithium-Ion Sieve Property of ≫-Type Manganese Oxide. *Solvent Extr. Ion Exch.* **1987**, *5* (3), 561–572.

(75) Xu, X.; Chen, Y.; Wan, P.; Gasem, K.; Wang, K.; He, T.; Adidharma, H.; Fan, M. Extraction of Lithium with Functionalized Lithium Ion-Sieves. *Prog. Mater. Sci.* **2016**, *84*, 276–313.

(76) Feng, Q.; Kanohb, H.; Ooib, K. *Materials Manganese Oxide Porous Crystals*.

(77) Hayashi, F.; Kurokawa, S.; Shiiba, H.; Wagata, H.; Yubuta, K.; Oishi, S.; Nishikiori, H.; Teshima, K. Exceptional Flux Growth and Chemical Transformation of Metastable Orthorhombic LiMnO2 Cuboids into Hierarchically-Structured Porous H1.6Mn1.6O4 Rods as Li Ion Sieves. *Cryst. Growth Des.* **2016**, *16* (11), 6178–6185.

(78) Wang, C.; Zhai, Y.; Wang, X.; Zeng, M. Preparation and Characterization of Lithium λ-MnO2 Ion-Sieves. *Front. Chem. Sci. Eng.* **2014**, *8* (4), 471–477.

(79) Yang, F.; Chen, S.; Shi, C.; Xue, F.; Zhang, X.; Ju, S.; Xing, W. A Facile Synthesis of Hexagonal Spinel λ-MnO2 Ion-Sieves for Highly Selective Li+ Adsorption. *Processes* **2018**, *6* (5).

(80) Wang, H.; Cui, J.; Li, M.; Guo, Y.; Deng, T.; Yu, X. Selective Recovery of Lithium from Geothermal Water by EGDE Cross-Linked Spherical CTS/LMO. *Chem. Eng. J.* **2020**, *389* (November 2019).

(81) Shen, X. M.; Clearfield, A. Phase Transitions and Ion Exchange Behavior of Electrolytically Prepared Manganese Dioxide. *J. Solid State Chem.* **1986**, *64* (3), 270–282.

(82) Biswal, A.; Tripathy, B. C.; Sanjay, K.; Subbaiah, T.; Minakshi, M. Electrolytic Manganese Dioxide (EMD): A Perspective on Worldwide Production, Reserves and Its Role in Electrochemistry. *RSC Adv.* **2015**, *5* (72), 58255–58283.

(83) Biswal, A.; Tripathy, B. C.; Sanjay, K.; Subbaiah, T.; Minakshi, M. Electrolytic Manganese Dioxide (EMD): A Perspective on Worldwide Production, Reserves

and Its Role in Electrochemistry. *RSC Adv.* **2015**, *5* (72), 58255–58283.

(84) Manuscript, A.; Society, R.; Manuscripts, A.; Manuscript, T. A.; Manuscripts, A.; Society, R.; Manuscript, A. RSC Advances.

(85) Ruetschi, P. Cation-Vacancy Model for Mn02. No. 43.

(86) Jung, W. Il; Nagao, M.; Pitteloud, C.; Itoh, K.; Yamada, A.; Kanno, R. Chemically Oxidized γ-MnO2 for Lithium Secondary Batteries: Structure and Intercalation/Deintercalation Properties. *J. Mater. Chem.* **2009**, *19* (6), 800–806.

(87) Vasiliev, I.; Magar, B. A.; Duay, J.; Lambert, T. N.; Chalamala, B. Ab Initio Studies of Hydrogen Ion Insertion into β-, R-, and γ-MnO 2 Polymorphs and the Implications for Shallow-Cycled Rechargeable Zn/MnO 2 Batteries . *J. Electrochem. Soc.* **2018**, *165* (14), A3517–A3524.

(88) Devaraj, S.; Munichandraiah, N. Effect of Crystallographic Structure of MnO2 on Its Electrochemical Capacitance Properties. *J. Phys. Chem. C* **2008**, *112* (11), 4406–4417.

(89) Minakshi, M.; Singh, P.; Issa, T. B.; Thurgate, S.; De Marco, R. Lithium Insertion into Manganese Dioxide Electrode in MnO2/Zn Aqueous Battery: Part III. Electrochemical Behavior of γ-MnO2 in Aqueous Lithium Hydroxide Electrolyte. *J. Power Sources* **2006**, *153* (1), 165–169.

(90) Chu, H. T.; Taylor, S. E. An Experimental Demonstration of a Multi-Element Flame Photometer: Determination of Salt Concentration in Soy Sauce. *Int. J. Chem.* **2015**, *8* (1), 25.

(91) Zhang, H.; Wu, A.; Fu, H.; Zhang, L.; Liu, H.; Zheng, S.; Wan, H.; Xu, Z. Efficient Removal of Pb(II) Ions Using Manganese Oxides: The Role of Crystal Structure. *RSC Adv.* **2017**, *7* (65), 41228–41240.

(92) Kim, C. H.; Akase, Z.; Zhang, L.; Heuer, A. H.; Newman, A. E.; Hughes, P. J. The Structure and Ordering of ε-MnO2. *J. Solid State Chem.* **2006**, *179* (3), 753–

774.

(93) Bakiro, M.; Hussein Ahmed, S.; Alzamly, A. Effect of PH, Surfactant, and Temperature on Mixed-Phase Structure and Band Gap Properties of BiNbO4 Nanoparticles Prepared Using Different Routes. *Chemistry (Easton).* **2019**, *1* (1), 89–110.

(94) Nie, J.; Yao, Z.; Shao, P.; Jing, Y.; Bai, L.; Xing, D.; Yi, G.; Li, D.; Liu, Y.; Yang, L.; Yu, K.; Luo, X. Revisiting the Adsorption of Antimony on Manganese Dioxide: The Overlooked Dissolution of Manganese. *Chem. Eng. J.* **2022**, *429* (September), 132468.

(95) Liu, B.; Zhang, Y.; Lu, M.; Su, Z.; Li, G.; Jiang, T. Extraction and Separation of Manganese and Iron from Ferruginous Manganese Ores: A Review. *Miner. Eng.* **2019**, *131* (248), 286–303.

(96) Zahid, M.; Abd-Elsalam, K. A. *Applications of Nanomaterials in Water Remediation: A Note from the Editors*; Elsevier Inc., 2021.

(97) Samadiy, M.; Deng, T. Lithium Recovery from Water Resources by Ion Exchange and Sorption Method. *J. Chem. Soc. Pakistan* **2021**, *43* (4), 406–416.

(98) Özmal, F.; Erdoɬan, Y. Li+ Adsorption/Desorption Properties of Lithium Ion-Sieves in Aqueous Solution and Recovery of Lithium from Borogypsum. *J. Environ. Chem. Eng.* **2015**, *3* (4), 2670–2683.

(99) Nandiyanto, A. B. D.; Ragadhita, R.; Yunas, J. Adsorption Isotherm of Densed Monoclinic Tungsten Trioxide Nanoparticles. *Sains Malaysiana* **2020**, *49* (12), 2881–2890.

(100) Park, H. J.; Singhal, N.; Jho, E. H. Lithium Sorption Properties of HMnO in Seawater and Wastewater. *Water Res.* **2015**, *87*, 320–327.

(101) Hormati, A.; Rezai, B.; Shoormasti, H. H.; Paydar, G. R. Extraction of Lithium Ions from Salt Lake Brine Using Magnetic Ionic Liquid: Kinetic and Equilibrium

Studies. *Inorg. Chem. Commun.* **2022**, 109693.

(102) Kalak, T.; Tachibana, Y. Removal of Lithium and Uranium from Seawater Using Fly Ash and Slag Generated in the CFBC Technology †. **2021**.

(103) Zhu, S. G.; He, W. Z.; Li, G. M.; Zhou, X.; Zhang, X. J.; Huang, J. W. Recovery of Co and Li from Spent Lithium-Ion Batteries by Combination Method of Acid Leaching and Chemical Precipitation. *Trans. Nonferrous Met. Soc. China (English Ed.* **2012**, *22* (9), 2274–2281.